NMR Study of the Heavy Fermion Compounds Yb-monopnictides

Kenjiro Hashi

1998

Contents

Chapter 1 Introduction

1.1 Introduction

In many rare-earth and actinide compounds, it has been thought that f-electrons are well localized in atoms due to the outer closed shell of p- and d-electrons. However, in Ce, Sm, Yb and U compounds, there are many anomalous properties which cannot be explained by a simple localized f-electron model. The most typical phenomena are Kondo effect and the formation of the heavy Fermion state. In these system, f-electrons fluctuate in space and time through the mixing with conduction electrons. In this chapter, we survey the Kondo effect and refer to the motivation of this study.

1.2 Kondo Effect

1.2.1 Impurity Kondo Effect

The Kondo effect was first found in alloys with transition metal as impurities. Figure 1-1 shows the temperature dependence of resistivity in CuFe alloys.[1-1] In these alloys, the resistivity shows a minimum with decreasing temperature and reaches a constant value called an unitarity limit. The minimum in the temperature dependence of resistivity was known by the 1930s, but it had remained unexplained for about 30 years. Then, it was explained by Kondo in 1964.[1-2] He calculated the scattering probability of the conduction electrons to the second Born approximation based on the s-d interaction model expressed by eq.(1-1) and showed that the resistivity proportional to -logT appears. The s-d interaction Hamiltonian is written as follows,

$$H=-J_{s\text{-}d}\, v\, \delta(r)\, (S \bullet s), \tag{1-1}$$

where v is the volume per lattice point, r is the position of the conduction electron and S and s are spins of the conduction electron and the impurity, respectively. The strength of the Kondo effect is characterized by the Kondo temperature T_K given by

$$k_B\, T_K = D \exp\left(-\frac{N}{|J_{s-d}|\, \rho}\right), \tag{1-2}$$

where D is the width of the conduction band, N is the number of lattice points and ρ is the density of states at the Fermi level.

Though the minimum of resistivity was explained by the appearance of the term proportional to -logT, an new problem about a ground state arose. The term of -logT diverges in the limit of T->0. Further, resistivity diverges at Kondo temperature T_K even in the case of the approximation of collecting the most divergent terms due to the higher perturbation. Thus, a perturbation theory is not proper below T_K. By the extensive theoretical investigations, the properties of the ground state of an alloy with an impurity are well understood: a spin of impurity is screened by spins of conduction electrons and a singlet ground state is formed by coupling an impurity spin with conduction electrons spins through the s-d interaction.[1-3] Thus, the Kondo effect makes a ground state to be nonmagnetic.

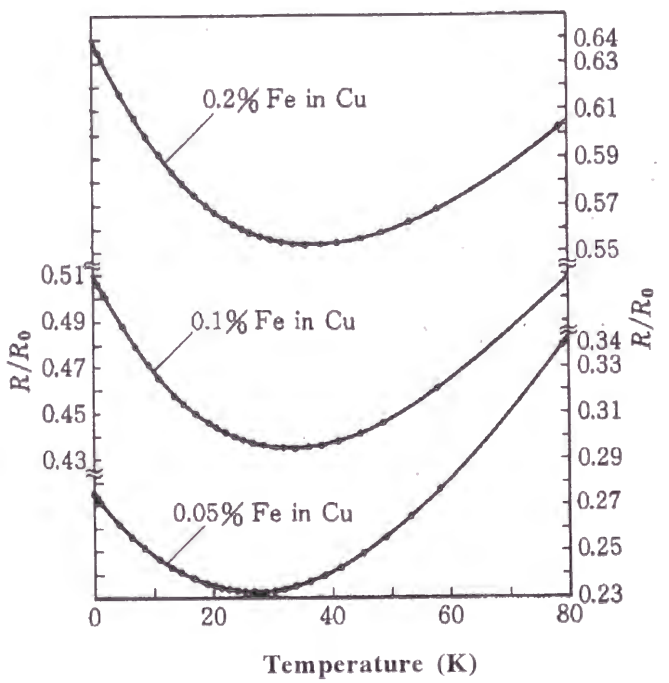

Fig. 1-1. Temperature dependence of resistivities in CuFe alloys.[1-1]

On the other hand, the above Kondo behavior such as the resistance minimum is observed in alloys with transition metal impurities of much less than 1 %. In alloys with transition metal impurities of more than a few percent, no Kondo behavior is observed and a magnetic phase transition such as spin glass occurs due to the RKKY interaction between localized moments mediated by conduction electrons. The RKKY interaction is

expressed as follows,

$$H=-J_{RKKY}\, S_1 \bullet S_2, \qquad (1\text{-}3)$$

where J_{RKKY} is an exchange integral and S_1 and S_2 are spins of localized moments. Thus, the RKKY interaction makes a system to have a magnetic phase transition.

The Kondo behavior is observed in some f-electron systems though magnetic moments form a lattice. In the next section, we turn to survey a dense Kondo effect.

1.2.2 Dense Kondo Effect

As mentioned in the previous section, the Kondo behavior in alloys with transition metal impurities appears only when the concentration of impurities is much less than 1 %. However, the Kondo behavior is observed in some f-electron systems though magnetic moments form a lattice. Below we survey the Kondo behavior referring the experimental results of $Ce_xLa_{1-x}Cu_6$ system as an example.[1-4,1-5] In Fig. 1-2, we show the temperature dependence of resistivities in $Ce_xLa_{1-x}Cu_6$ system. In the compound with x=0.094, the impurity Kondo behavior is observed: the resistivity has a minimum around 25 K and it is proportional to -logT between 2 K and 20 K, and takes a constant value below 0.1 K. These Kondo behavior is also observed even in the compound with x=1: the resistivity has a minimum at about room temperature and proportional to -logT between 30 K and 100 K. This Kondo effect in f-electron compound is referred to as a dense Kondo effect in contrast to an impurity Kondo effect.

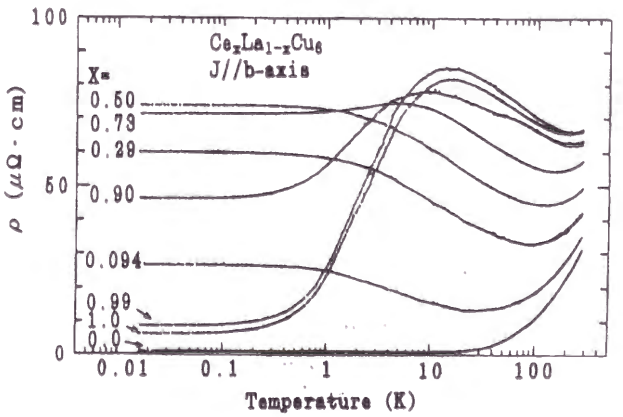

Fig. 1-2. Temperature dependence of resistivities in $Ce_xLa_{1-x}Cu_6$ system.[1-4]

The temperature dependence of the resistivity in the compound with x>0.73 is different from that in the compound with x<0.50: the resistivity has a maximum and decreases with decreasing temperature below about 10 K. In this temperature range, the decrease of resistivity follows T^2 dependence and is regarded as a formation of a coherent state and/or a heavy Fermion state. The susceptibility shows large Pauli paramagnetism $\chi_{Pauli}(0)$ at T=0 K as shown in Fig 1-3. The coefficient γ of electric specific heat takes a large value as shown in Fig 1-4. These behavior is observed in many f-electron compounds. According to the Fermi liquid theory, susceptibility $\chi_{Pauli}(0)$ due to the Pauli paramagnetism and coefficient γ are expressed as follows,

$$\chi_{Pauli}(0) = 2\,\mu_B^2\,\rho(\varepsilon_F), \tag{1-4}$$

$$\gamma = \frac{\pi^2}{3} k_B^2\,\rho(\varepsilon_F), \tag{1-5}$$

where $\rho(\varepsilon_F)$ is a density of states at Fermi level. Thus, the enhancement of susceptibility and coefficient γ is regarded as the enhancement of the density of states at Fermi level and/or an effective mass of conduction electron. There is a linear relation between $\chi_{Pauli}(0)$ and A, where A is the coefficient of the T^2 term of the resistivity.[1-6] Further, there is a linear relation between A and γ^2.[1-7] Corresponding to the enhancement of $\rho(\varepsilon_F)$, the effective mass of quasi-particles in $CeCu_6$ is about 1000 times larger than that of free electron. Thus, this state is referred to as a heavy Fermion state. Here, it should be noted that susceptibility $\chi_{Pauli}(0)$ and coefficients γ per Ce ions in $Ce_xLa_{1-x}Cu_6$ system are almost the same above 10 K and 1 K, respectively. This means that the Kondo effect occurs at each Ce site independently even in a dense Kondo compound.

The dense Kondo compounds show various properties as well as heavy Fermion state. These compounds are classified as follows corresponding to those ground states: heavy Fermion state without magnetic orderings, with magnetic orderings, with superconducting and so on. These various ground states originate from the competition between the Kondo effect and the RKKY interaction. These behavior have not fully understood yet and attract much attention due to their anomalous properties as follows. In

compounds without magnetic orderings, development of correlation length is strongly suppressed by the Kondo effect. On the other hand, in compounds with magnetic orderings, magnetic transitions occur at very low temperatures compared to the exchange interactions between localized moments. Further, the value of ordered magnetic moments is reduced compared to the expected value without the Kondo effect in some compounds with magnetic orderings. The boundary between nonmagnetic and magnetic compounds is one of the most interesting topics.

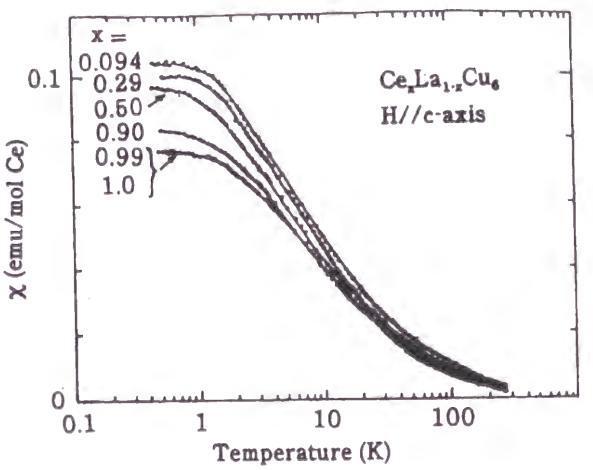

Fig. 1-3. Temperature dependence of magnetic susceptibilities in $Ce_xLa_{1-x}Cu_6$ system.[1-4]

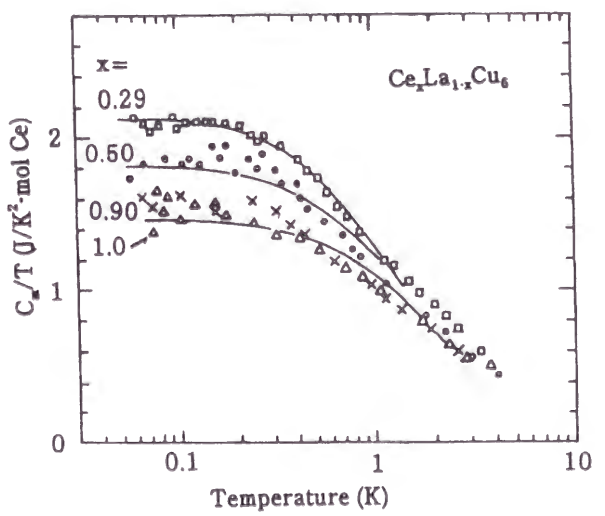

Fig. 1-4. Temperature dependence of specific heat derived temperature in $Ce_xLa_{1-x}Cu_6$ system.[1-5]

Another interesting topic is the Kondo behavior in low carrier systems. Usually in the Kondo system, the conduction electrons couple with each magnetic ion so as to screen the localized moment. Thus a substantial amount of conduction electrons are thought to be necessary for the heavy Fermion state. However, the Kondo behavior is observed in Yb_4As_3,[1-8] CeSb, CeBi[1-9] and so on, where the carrier concentration is less than a few percent per magnetic ion. The Yb-monopnictides, which we investigate in this study, belong to this category. In the next section, we survey the physical properties of Yb-monopnictides and discuss the motivation of this study.

1.3 Physical Properties of Yb-monopnictides

Yb-monopnictides YbX (X: N, P, As, Sb) have the cubic NaCl-type crystal structure and semi-metallic band structure as Ce-monopnictides. Figures 1-5(a), 1-5(b) and 1-5(c) show the band structure of LuP, LuAs and LuSb, respectively, calculated by Harima et al. including the spin-orbit interactions as perturbation.[1-10] The band structure shows that p-character holes which originate from pnictogen are around Γ point and that d-character electrons which originate from Lu atoms are around X point. The p-character holes are split into two states, p-Γ_6 and p-Γ_8 states by spin-orbit interactions. It is thought that the band structure of Yb-monopnictide is similar to that of Lu-monopnictide. This is supported by some experimental results on transport properties.[1-11] First, measurements of the Hall coefficients show that these systems have small amount of carriers. Second, the magneto-resistance of YbAs follows H^2 dependence. From these transport measurements, the number of carriers was estimated to be about 0.01 carriers per Yb^{3+} ion in YbAs. The Hund-rule ground-state multiplet of the $(4f)^{13}$ electric configuration, J=7/2 is split by a crystalline-electric-field (CEF) into a Γ_6 doublet as the ground state, a Γ_8 quartet and a Γ_7 doublet as the first and the second exited states. The energies of the excited states from the ground states are listed in Table 1-1.[1-12,1-13] The energies decrease systematically with changing the pnictogen from N to Sb.

		YbN	YbP	YbAs	YbSb
Γ_8-Γ_6 (K)	Ref. (1-12)	389	261	218	
	Ref. (1-13)	383	220	203	174
Γ_7-Γ_6 (K)	Ref. (1-12)	584	407	489	
	Ref. (1-13)	940	499	476	453

Table 1-1. Crystalline electric field splittings in Yb-monopnictides. [1-12,1-13]

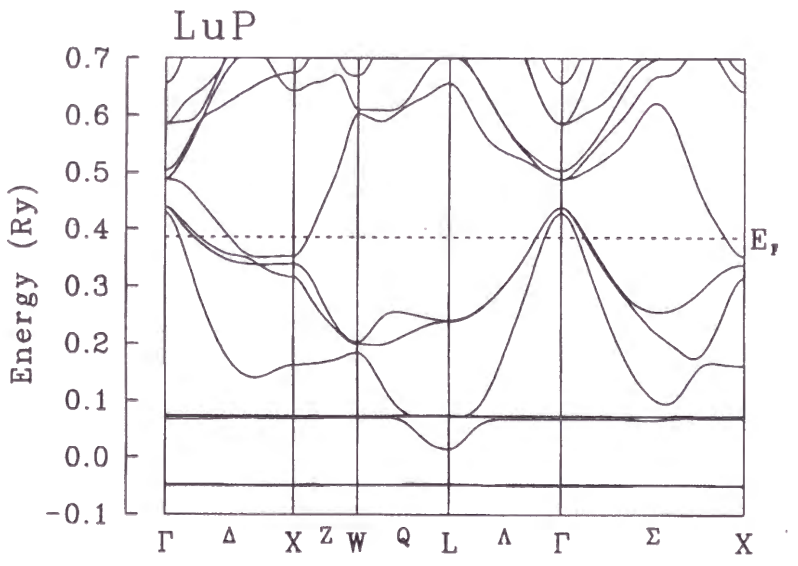

Fig. 1-5(a). Energy band structure calculated for LuP.[1-10]

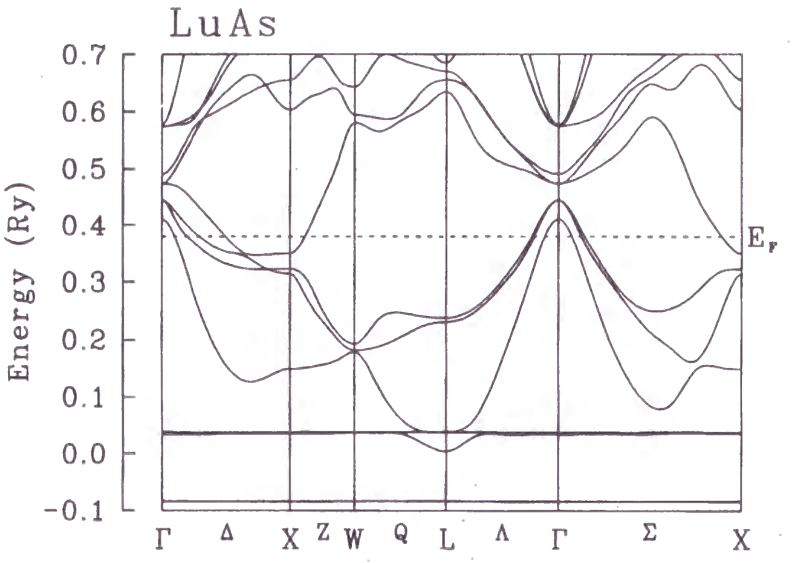

Fig. 1-5(b). Energy band structure calculated for LuAs.[1-10]

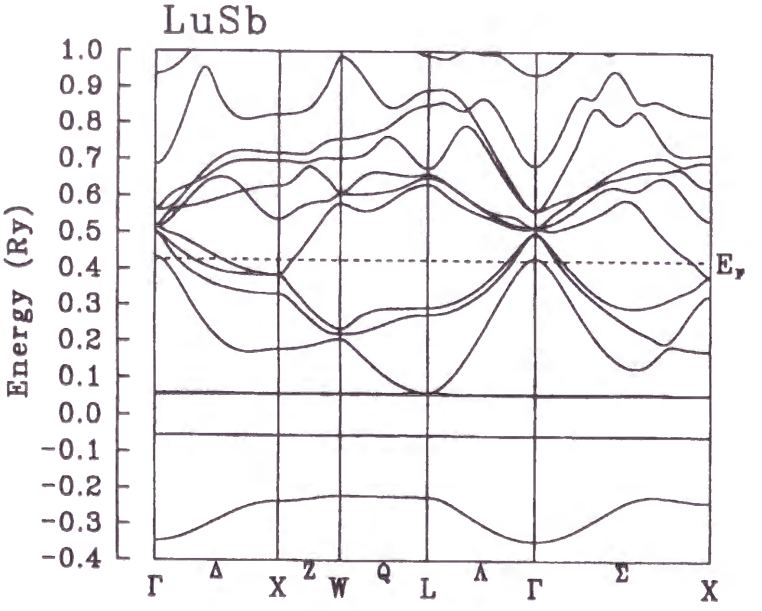

Fig. 1-5(c). Energy band structure calculated for LuSb.[1-10]

The first report on the anomalous behavior of Yb-monopnictides was one regarding the temperature dependence of the susceptibilities.[1-14] Figure 1-6 shows the temperature dependence of the susceptibilities of Yb-monopnictides. No magnetic transition is found down to 1.5 K, though the effective moment of these system above 80 K are almost same with that of the trivalent configuration of the Yb ion, and the absolute values of the Weiss temperatures are larger than 10 K. The susceptibility below about 70 K deviates from the behavior of a simple single ion model showing the smaller value.

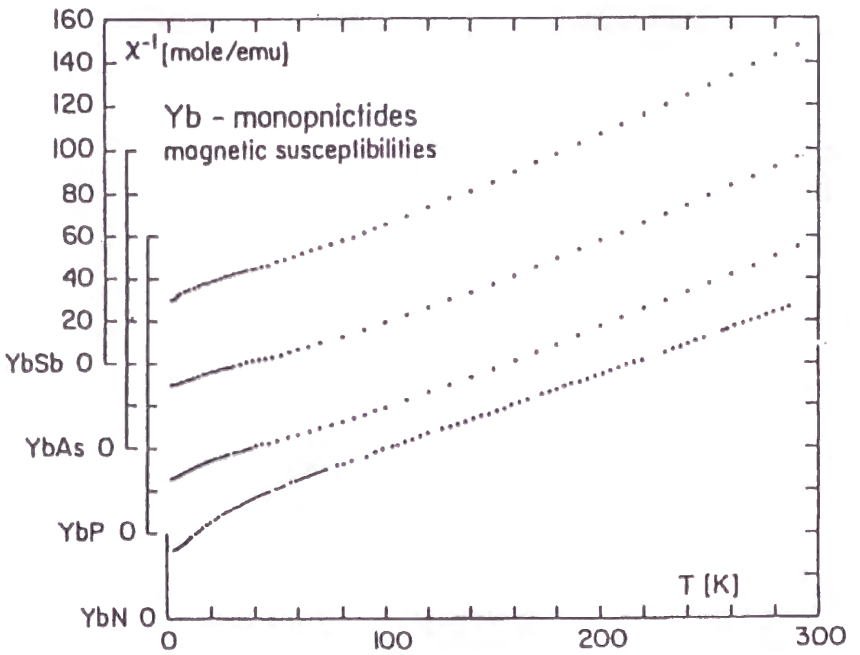

Fig. 1-6. Temperature dependence of magnetic susceptibilities in Yb-monopnictides.[1-14]

An anomalous behavior is also found in the specific heat. The specific heat shows a broad peak around 5 K, as shown in Fig. 1-7. This broad peak can not be explained by the Schottky peak, since the magnitude of the electric crystal field splitting is much larger. This peak is compared with the exact solution of the single impurity Kondo model as also shown by a solid line in Fig. 1-7.[1-15] The Kondo temperature is tentatively estimated to be 5.7 K. These behavior such as suppression of a magnetic ordering and a broad peak in specific heat is characteristic to the Kondo compounds. However, no Kondo behavior is found in the temperature dependence of resistivities of YbP and YbAs as shown in Figs. 1-8(a) and 1-8(b), respectively.[1-16] This discrepancy is explained by the p-f mixing model.[1-11] Yb-monopnictides have two types of carriers, holes and electrons, because they are compensated semimetalic compounds. The CEF ground state Γ_6 of 4f-electrons mixes with p-Γ_6 holes stronger than with d-character electrons due to their symmetry. Thus, it is thought that the Kondo effect occurs mainly through the mixing between 4f-electrons and p-Γ_6 holes. Mobility of conduction electrons is larger than that of holes as shown in Fig. 1-9. Thus, the Kondo behavior of resistivity can be masked by resistivity of the conduction electrons which are not affected by the Kondo effect. The dHvA measurements of YbAs show that there are both Fermi surfaces of holes and electrons.[1-17] However, not all of the Fermi surface of holes were observed. The holes which were not observed by dHvA measurements can be connected to the holes affected by Kondo effect.

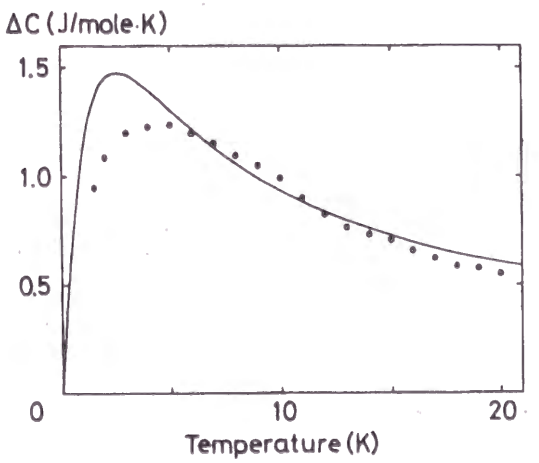

Fig. 1-7. Temperature dependence of magnetic specific heat in YbP.
The solid line shows the exact solution for the single impurity model. [1-15]

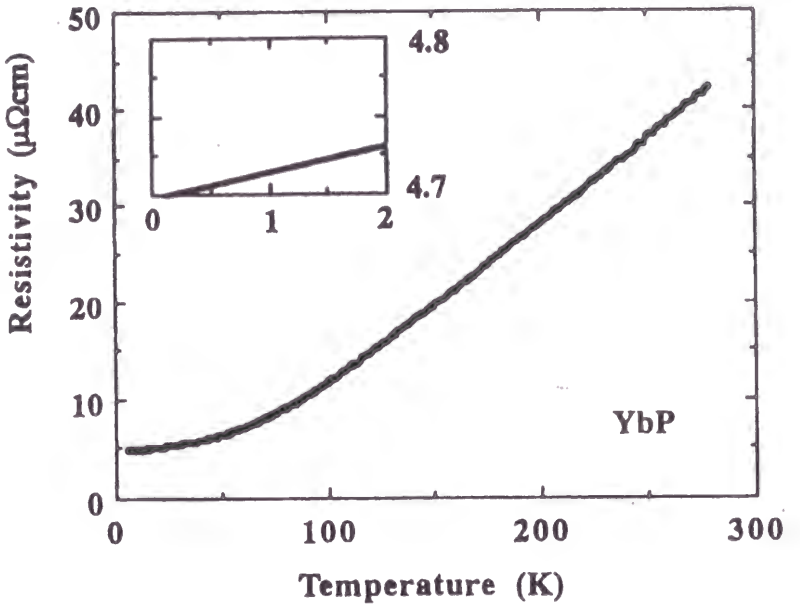

Fig. 1-8(a). Temperature dependence of resistivity in YbP. Insert shows the detail near T_N.[1-16]

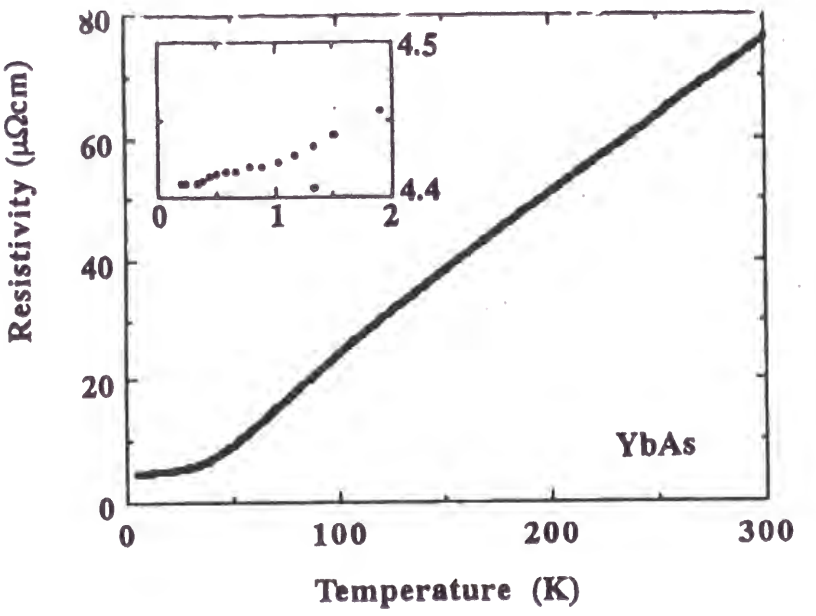

Fig. 1-8(b). Temperature dependence of resistivity in YbAs. Insert shows the detail near T_N.[1-16]

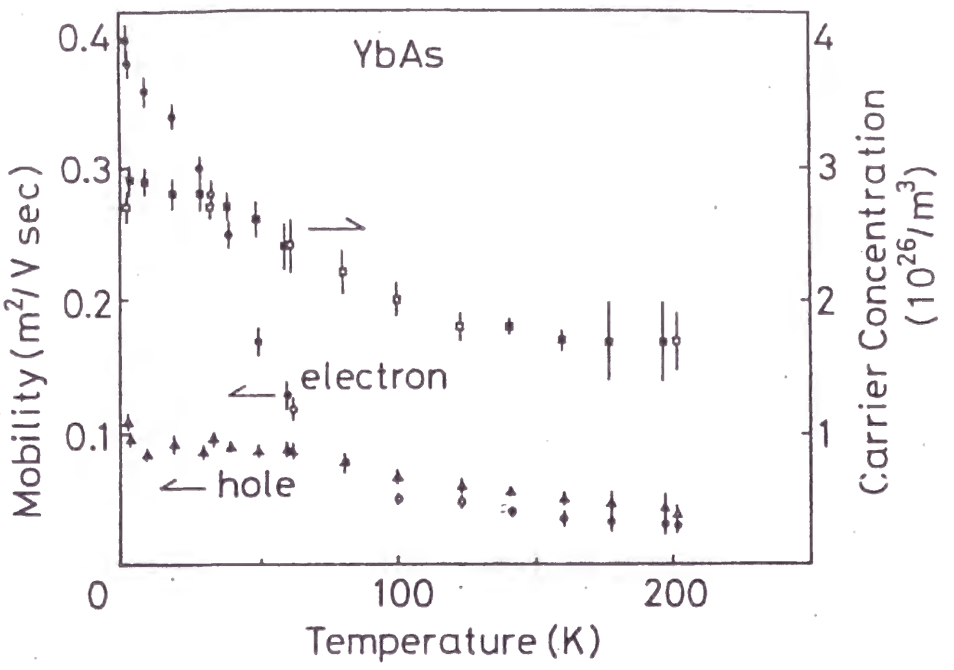

Fig. 1-9. Temperature dependence of both the mobilities of electrons and holes and the carrier number.[1-16]

Yb-monopnictides except YbSb undergo clear antiferromagnetic transitions below 1 K.[1-18] Figure 1-10 shows the temperature dependence of the specific heat of Yb-monopnictides. There is a sharp peak at about 0.5 K corresponding to the antiferromagnetic transition.

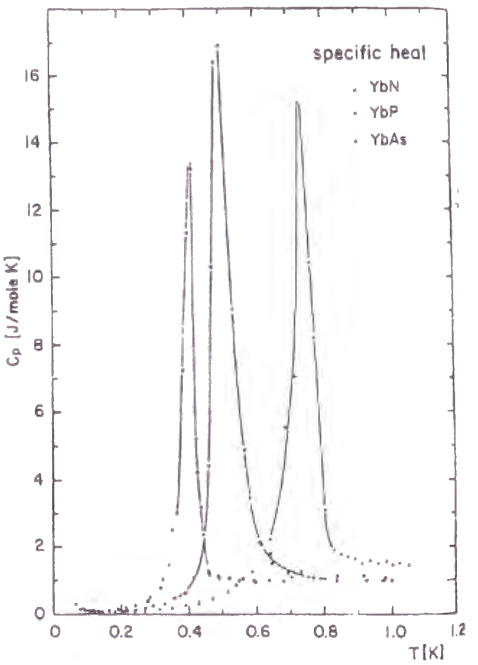

Fig. 1-10. Temperature dependence of Yb-monopnictides around T_N.[1-18]

From neutron diffraction measurements, it was reported that the magnetic structure of the ordered state is of Type II for YbP and of Type III for YbN and YbAs, whose propagation vectors are [1/2,1/2,1/2] and [1,0,1/2], respectively, and that the ordered magnetic moments are reduced by about half from the expected value for the Γ_6 ground state.[1-19] The reduction of ordered magnetic moments is quite similar to that in other heavy Fermion compounds and is observed only in Yb-monopnictides among low carrier concentration systems. Furthermore the coefficient γ of electronic specific heat in YbAs was estimated to be 270 mJ/mol K^2 by the specific heat measurement below T_N.[1-20] Inelastic neutron scattering studies showed that short-range spin correlations begin to develop below about 20 K far above T_N.[1-21] This is consistent with the fact that all the entropy of the ground state (R ln2) is released above 20 K, including the entropy corresponding to a broad maximum of specific heat around 5 K.[1-14] These experimental

results are again quite similar to other heavy Fermion compounds.

On the other hand, YbSb is an exceptional case in Yb-monopnictides. Neutron diffraction measurements on YbSb did not detect any magnetic moments larger than 0.1 μ_B down to 7 mK.[1-19] However, the Mössbauer measurements performed on the same sample with the neutron diffraction measurements reveal the existence of the two phase transition at 0.32 K and 5 K.[1-22] It was reported that the phase transition at 0.32 K is antiferromagnetic ordering and the transition at 5 K is possibly antiferroquadrupolar ordering. However, CEF ground state Γ_6 has no quadrupolar moment. Thus, the situation is not very clear so far. The transition at 5 K was detected by specific heat measurements as shown in Fig. 1-11.[1-23] These anomalous behavior in YbSb is consistent with the difference of the band structure. The number of the p-Γ_6 holes decreases with increasing the weight of pnictogen due to spin-orbit interactions. In YbSb, it is expected that the number of p-Γ_6 holes is almost zero. Thus, the p-f mixing model cannot be applied to YbSb and a new model is required to understand the physical properties in Yb-monopnictides systematically.

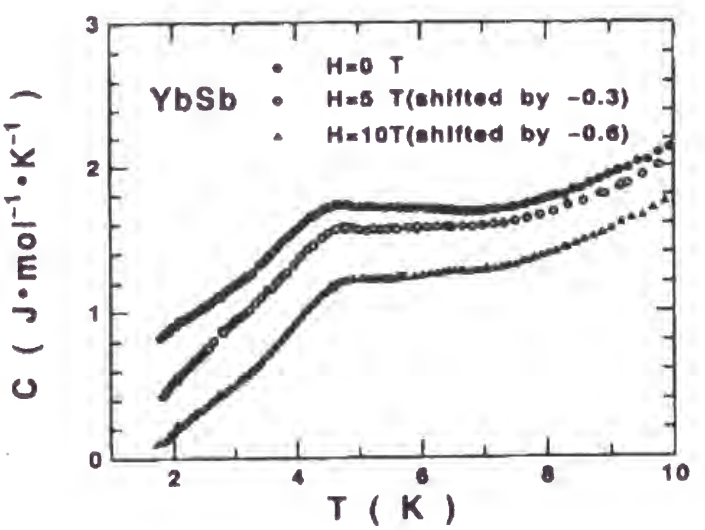

Fig. 1-11. Temperature dependence of specific heat in YbSb under magnetic field of 0, 5, 10 T.[1-23]

1.4 Motivation of This Study

Yb-monopnictides have many similarities with usual heavy Fermion compounds as mentioned above. However, it has been controversial that the heavy Fermion state can be realized in the low carrier concentration system. There has been a suggestion that the observed T-linear specific heat in YbAs is not due to heavy Fermion state, but due to the magnons of which the density of state is proportional to the energy.[1-24] Very recently it was also suggested that the charge dipolar model may explain the above mentioned experimental results.[1-25] Thus the interpretation for the magnetic properties of Yb-monopnictides is unsettled and it has been controversial that the magnetic properties in Yb-monopnictides can be understood by considering the existence of the heavy Fermion state or by a different mechanism.

In this study, we have performed the nuclear magnetic resonance and relaxation measurements of Yb-monopnictides to clarify the physical properties from the microscopic standpoint. In particular, YbAs has been investigated at low temperatures down to 20 mK. Further, we put an emphasis on YbSb to clarify an ambiguous situation that whether a phase transition at about 5 K exists or not.

In chapter 2, we present sample preparation and experimental methods. Experimental results are given in chapter 3. In chapter 4, we analyze the experimental results and discuss the physical properties of Yb-monopnictides. Then, we present conclusions in chapter 5.

References

(1-1) J. P. Franck, F. D. Manchester and D. L. Martin: Proc. Roy. Soc. A263 (1961) 494.

(1-2) J.Kondo: Prog. Theor. Phys. 32 (1964) 37.

(1-3) K. Yoshida and A. Yoshimori: Magnetism V, ed. by H. Suhl (Academic Press, 1973).

(1-4) A. Sumiyama, Y. Oda, H. Nagano, Y. Ōnuki, K. Shibutani and T. Komatsubara: J. Phys. Soc. Jpn. 55 (1986) 1294.

(1-5) K. Satoh, T. Fujita, Y. Maeno, Y. Ōnuki and T. Komatsubara: J. Phys. Soc. Jpn. 58 (1989) 1012.

(1-6) P. A. Lee, T. M. Rice, J. W. Serene, L. J. Sham and J. W. Wilkins: Comments on Condensed Matter Physics, 12 (1986) 99.

(1-7) K. Kadowaki and S. B. Woods: Solid State Communi. 58 (1986) 507.

(1-8) A. Ochiai, T. Suzuki and T. Kasuya: J. Phys. Soc. Jpn. 59 (1990) 4129.

(1-9) T. Kasuya, K. Takegahara, Y. Aoki, T. Suzuki, S. Kunii, M. Sera, N. Sato, T. Fujita, T. Goto, A. Tamaki and T. Komatsubara: Valence Instabilities, ed. P. Wachter and H. Boppart (North-Holland Publishing Company, 1982) p. 359.

(1-10) H. Harima: private communication.

(1-11) A. Oyamada, C. Ayache, T. Suzuki, J. Rossat-Mignod and T. Kasuya: J. Magn. Magn. Mater. 90&91 (1990) 443.

(1-12) M. Kohgi, K. Ohoyama, A. Oyamada, T.Suzuki and M. Arai: Physica B 163 (1990) 625.

(1-13) A. Dönni, A. Furrer, P. Fischer, F. Hulliger and P. Wachter: Physica B 171 (1991) 353.

(1-14) H. R. Ott, F. Hulliger and H. Rudigier: Valence Instabilities, ed. P. Wachter and H. Boppart (North-Holland Publishing Company, 1982) p. 551.

(1-15) S. Takagi, A. Oyamada and T. Kasuya: J. Phys. Soc. Jpn. 57 (1988) 1456.

(1-16) A. Oyamada: Dr. Thesis, Department of Physics, Tohoku University, 1991.

(1-17) N. Takeda, K. Tanaka, M. Kagawa, A. Oyamada, N. Sato, S. Sakatsume, H. Aoki, T. Suzuki and T. Komatsubara: J. Phys. Soc. Jpn. 62 (1993) 2098.

(1-18) H. R. Ott, H. Rudigier and F. Hulliger: Solid State Communi. 55 (1985)

113.

(1-19) A. Dönni, A. Furrer, P. Fischer, F. Hulliger, P. Wachter and H. R. Ott: J. Magn. Magn. Mater. 90&91 (1990) 143.

(1-20) T. Sakon, N. Sato, A. Oyamada, N. Takeda, T. Suzuki and T. Komatsubara : J. Phys. Soc. Jpn. 61 (1992) 2209.

(1-21) K. Ohoyama, T. Osakabe, A. Dönni, M. Kohgi, A.Oyamada and T. Suzuki: Physica B 213&214 (1995) 119.

(1-22) P. Bonville, J. A. Hodges, F. Hulliger, P. Imbert, G. Jéhanno, J. B. Marimon da Cunha and H. R. Ott: J. Magn. Magn. Mater. 76&77 (1988) 473.

(1-23) D. X. Li, A. Oyamada, H. Shida, T. Suzuki, T. Kasuya, A. Dönni and F. Hulliger: Physica B 186-188 (1993) 547.

(1-24) T. Kasuya: J. Phys. Soc. Jpn. 63 (1994) 843.

(1-25) T. Kasuya and D. X. Li: J. Phys. Soc. Jpn. 66 (1997) 1587.

Chapter 2 Experimental Procedure

2.1 Sample Preparation

In this study, we have performed NMR measurements on six kinds of Yb-monopnictides including $YbP_{0.4}As_{0.6}$ and $YbAs_{0.8}Sb_{0.2}$ alloys. In the following, we describe the preparing methods of single or powder Yb-monopnictides samples.

Single crystals of YbP, YbAs and $YbAs_{0.8}Sb_{0.2}$ were grown by two stage procedures. Firstly, the stoichiometric quantities of elements Yb (3N pure), P (6N pure), As (6N pure) and Sb (6N pure) were sealed in an evacuated quartz tube and were heated up to 700 °C taking a few weeks. Then powder samples were prepared through the reaction between metallic Ytterbium filings and the vapor of pnictogens. Secondly, the Bridgman method in a sealed tungsten crucible was used to obtain a single crystal. For NMR measurements, the single crystal was ground into fine powders to avoid skin effect.

Powder samples of $YbP_{0.4}As_{0.6}$ were prepared by the same procedure of the first stage for preparing the single crystals.

YbSb is the only incongruent compound in Yb-monopnictides. Thus, its synthesis is very difficult. Only the powder samples of YbSb can be prepared by the same procedure of the first stage for preparing the single crystals of the other Yb-monopnictides at the temperature just below the incongruent melting point of about 800 °C. In this study, we have used the both samples prepared by the ETH group and by us. From now on, we refer to the samples prepared by the ETH group and by us as YbSb#1 and YbSb#2, respectively. The difference between YbSb#1 and YbSb#2 is discussed below.

Powder samples of YbN were prepared by heating metallic Ytterbium filings up to about 1600 °C in hydrostatic N_2 gas pressure of about 1000 atms. In this study, we have used the powder samples of YbN prepared by D. X. Li et al.

Each sample prepared by the above procedures was checked by X-ray diffraction. All sample except YbSb were found to be single phases. The crystal structure was found to be NaCl-type and the lattice constants were obtained as follows: 5.55 Å for YbP, 5.63 Å for $YbP_{0.4}As_{0.6}$, 5.70 Å for YbAs and 5.72 Å for $YbAs_{0.8}Sb_{0.2}$. These values are almost the same with those obtained by the previous study for YbP and YbAs and the Vegard's rule for the alloys. On the other hand, YbSb has some impurity phases. Figure

2-1 shows the X-ray diffraction pattern of YbSb#2. Sharp peaks indexed by the letters of YbSb show that the crystal structure is NaCl-type and the lattice constant is 6.07 Å, which is almost the same with that of YbSb#1. However, some small impurity peaks, which may come from Yb_5Sb_4 and/or $Yb_{11}Sb_{10}$, were found around 2θ=32 degree. These small peaks were also found in YbSb#1. The ratio of intensity between the peaks corresponding to the YbSb {200} plane and the impurity Yb_5Sb_4 {330} plane in YbSb#2 is as small as 10 : 1, which is almost the same with that in YbSb#1. However, the width of the peak corresponding to the YbSb {220} plane in YbSb#2 is about a half of that in YbSb#1. Thus, it is found that the homogeneity in YbSb#2 is better than that in YbSb#1.

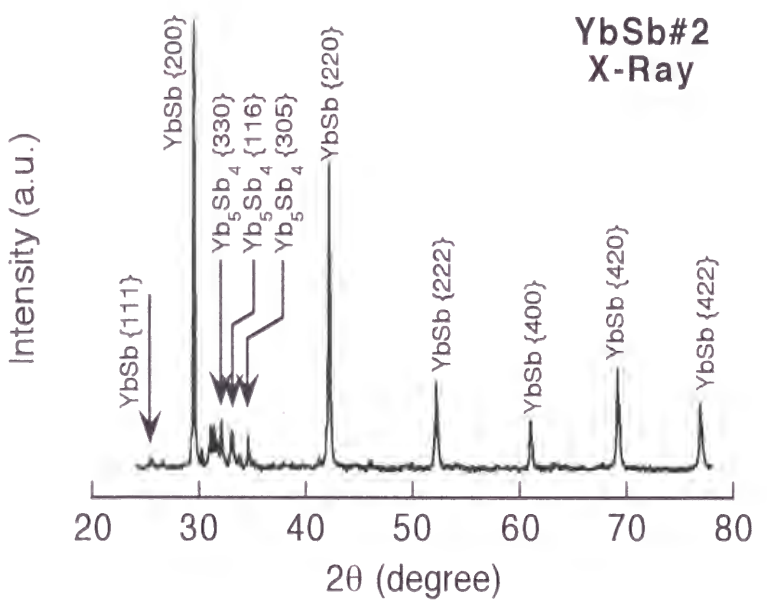

Fig. 2-1 X-ray diffraction pattern of YbSb#2.

2.2 *NMR Measurements*

NMR measurements on pnictogens were performed using a conventional phase-coherent pulsed spectrometer. Figure 2-2 shows a block diagram of the NMR apparatus. NMR spectra were obtained by the observation of the spin echo intensity as a function of external magnetic field. Knight shifts were obtained by using the gyromagnetic ratios of 3.0756 (MHz/10 kOe), 17.235 (MHz/10 kOe), 7.2919 (MHz/10 kOe) and 10.189 (MHz/10 kOe) for ^{14}N, ^{31}P, ^{75}As and ^{121}Sb, respectively. The magnitude of magnetic field was measured by a Hall resistance which was calibrated by the reference signal of ^{11}B in Triethyl Borate $(CH_3CH_2O)_3B$ assuming the gyromagnetic ratio of 13.660 (MHz/10 kOe). The spin-lattice relaxation time T_1 was measured by observing the recovery of spin-echo intensity after the saturation of nuclear magnetization by saturating comb pulses. The schematic view of pulse sequence for the measurement of T_1 is shown in Fig 2-3. The recovery of spin-echo intensity is expressed as follows,

$$M(t) = M_0\{1 - \exp(-\frac{t}{T_1})\}, \qquad (2\text{-}1)$$

where M(t) is the spin-echo intensity at the time t after the saturation comb pulses and M_0 is that of equilibrium.

The resonance frequency ranged from about 5 MHz to about 60 MHz.

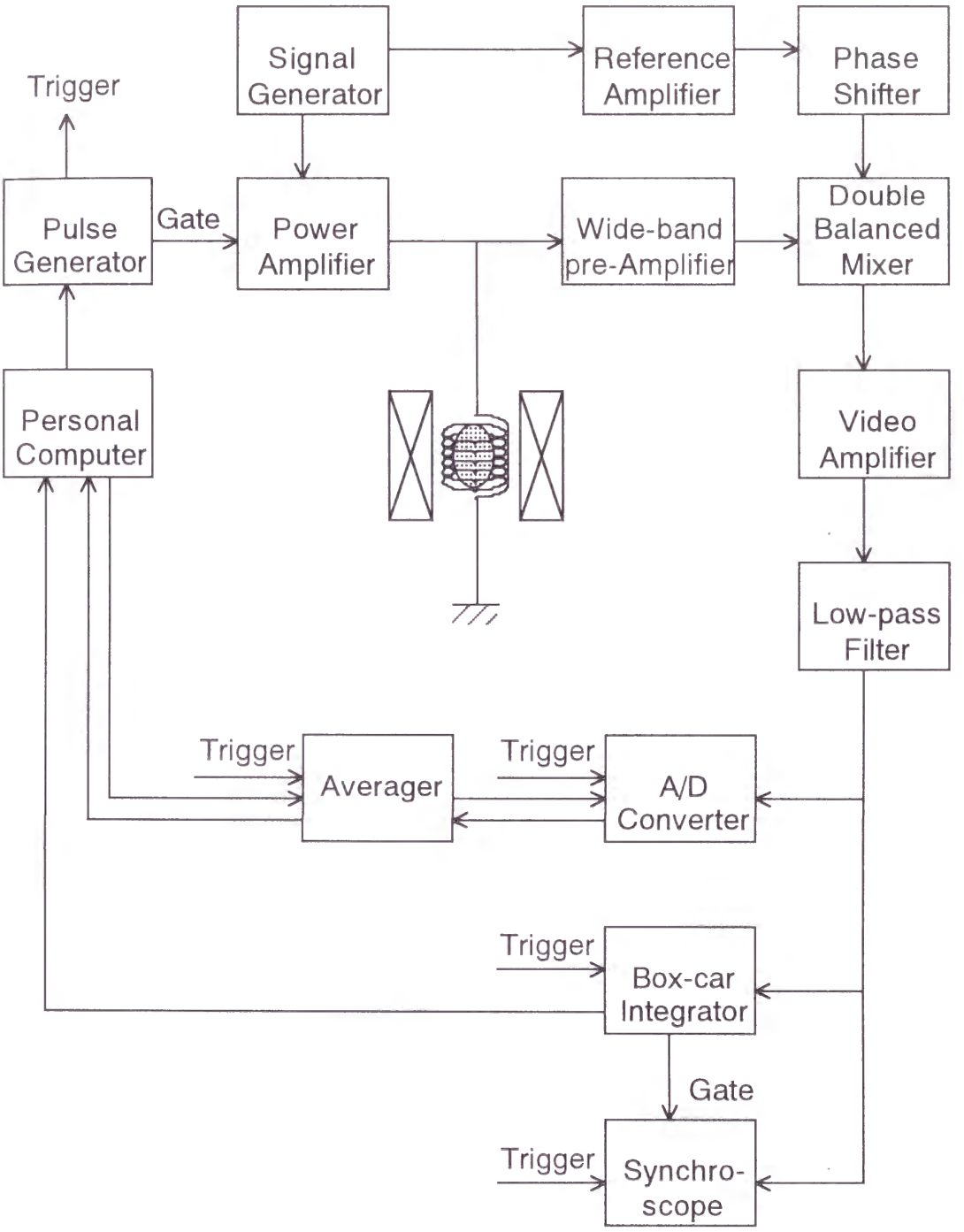

Fig. 2-2 Block diagram of phase-coherent pulsed NMR spectrometer.

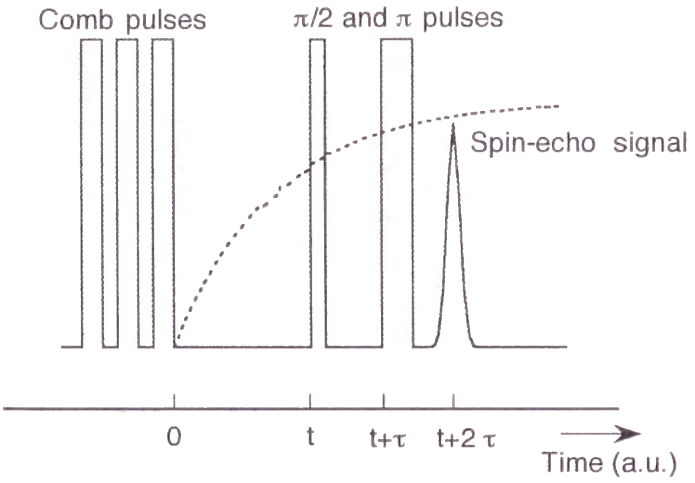

Fig. 2-3. The schematic view of pulse sequence for the measurement of T_1

2.3 ^{3}He-^{4}He Dilution Refrigerator

The temperature below 1.2 K was obtained by using a ^{3}He-^{4}He dilution refrigerator. This refrigerator use large entropy of liquid ^{3}He by diluting liquid ^{3}He with liquid ^{4}He. The schematic view of ^{3}He-^{4}He dilution refrigerator is shown in Fig. 2-4.

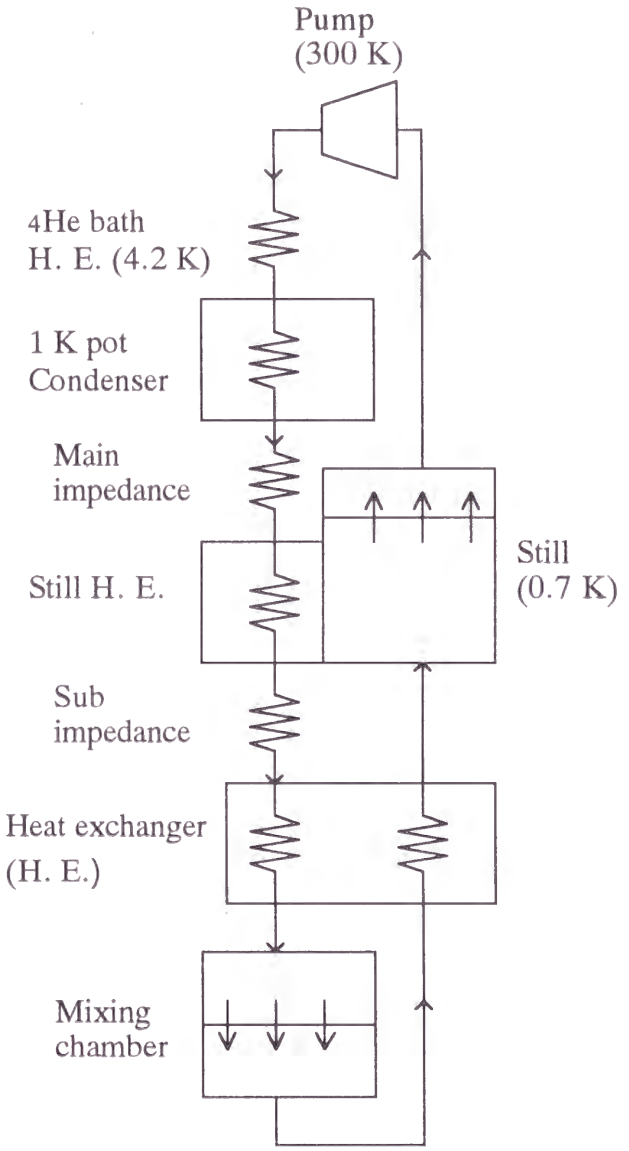

Fig. 2-4 The schematic view of ^{3}He-^{4}He dilution refrigerator

Chapter 3 Experimental Results

3.1 Paramagnetic State

3.1.1 NMR spectrum and Knight Shifts

First we show the experimental results in the paramagnetic state. A single Lorentzian-typed NMR spectrum was observed above 1.5 K in all Yb-monopnictides. Figure 3-1 shows a typical example of the NMR spectra in the paramagnetic state. No structure due to the electric quadrupole moments was observed, although nuclear spins of ^{14}N, ^{75}As and ^{121}Sb is 1, 3/2 and 5/2, respectively. This indicates that the local symmetry of the pnictogen site is cubic, which is expected from the NaCl-type crystal structure, and that there is no distortion in the sample.

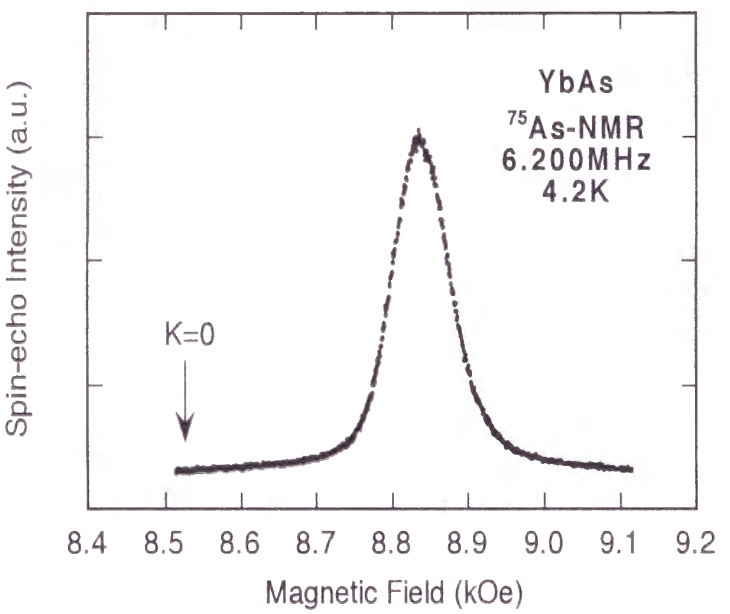

Fig. 3-1. A typical example of the NMR spectrum in the paramagnetic state.

The Knight shifts K(T) was measured using these spectra. The Knight shifts K(T) measured at a constant frequency is usually defined as follows:

$$K(T) = \frac{H_0 - H_m(T)}{H_m(T)}, \qquad (3\text{-}1)$$

where H_0 is the resonant external magnetic field of the free pnictogen nuclei and $H_m(T)$ is the observed resonant external magnetic field.

Figures 3-2, 3-3, 3-4 and 3-5 show the temperature dependence of the Knight shifts K(T) for YbN, YbP, YbAs and YbSb, respectively. We also show the temperature dependence of K(T) for $YbP_{0.4}As_{0.6}$ measured by using ^{31}P and ^{75}As nuclei as a probe in Figs. 3-6(a) and 3-6(b), respectively. The NMR signal of ^{75}As nuclei in $YbP_{0.4}As_{0.6}$ was observed only below about 20 K due to their week intensity. We show the temperature dependence of K(T) for $YbAs_{0.8}Sb_{0.2}$ measured by using ^{75}As nuclei as a probe in Fig. 3-7. The NMR signal of ^{121}Sb nuclei in $YbAs_{0.8}Sb_{0.2}$ was not observed due to their week intensity.

The sign of the observed Knight shift is negative in the all temperature range. The absolute value becomes large with decreasing temperature. The Knight shift K(T) is almost temperature independent below 4.2 K.

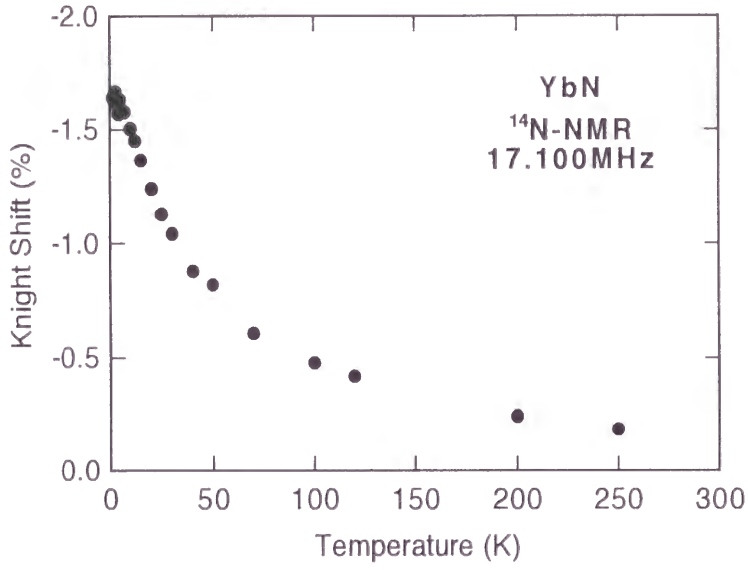

Fig. 3-2. Temperature dependence of the Knight Shift of YbN.

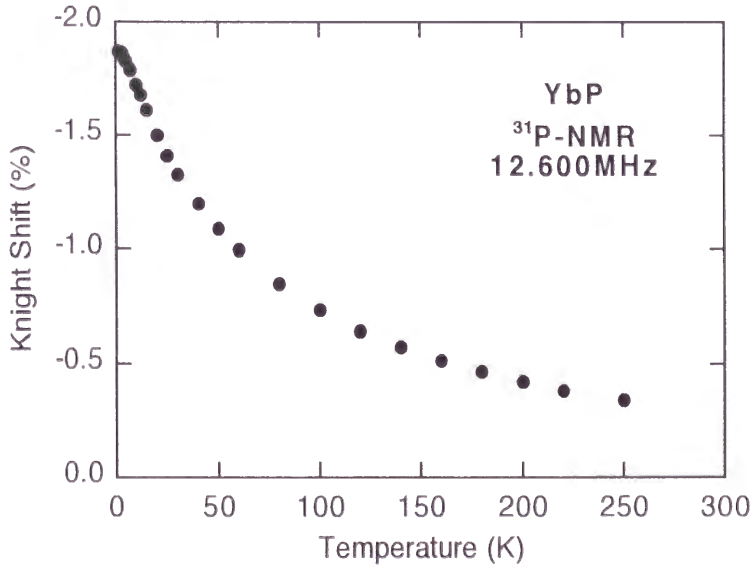

Fig. 3-3. Temperature dependence of the Knight Shift of YbP.

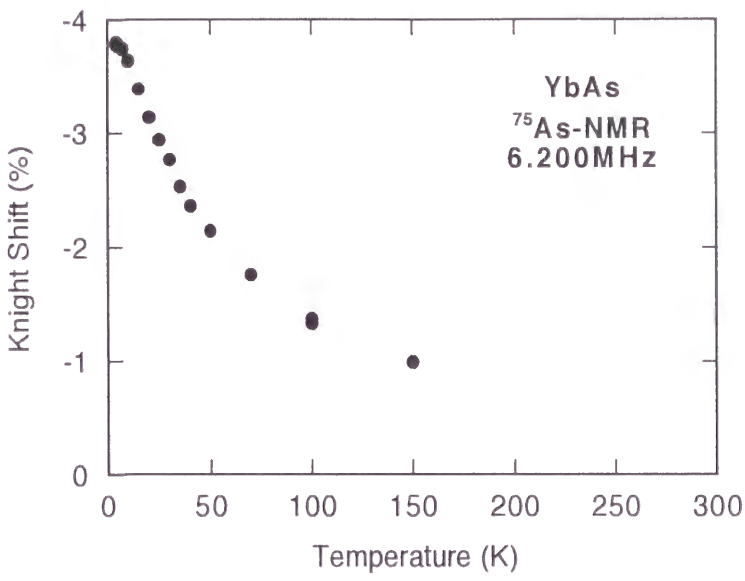

Fig. 3-4. Temperature dependence of the Knight Shift of YbAs.

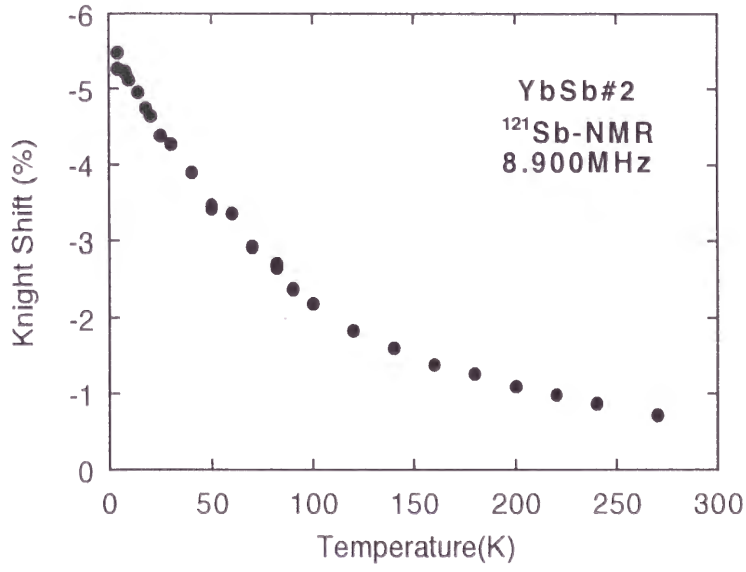

Fig. 3-5. Temperature dependence of the Knight Shift of YbSb.

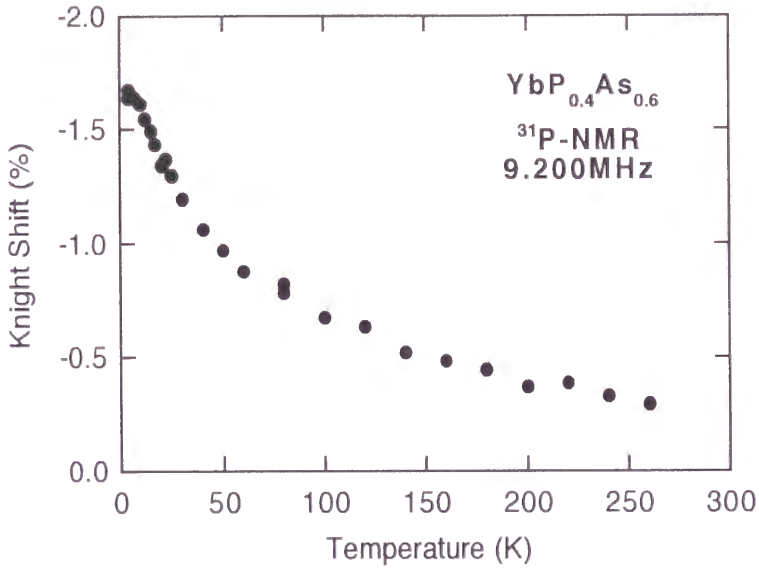

Fig. 3-6(a). Temperature dependence of the Knight Shift of $YbP_{0.4}As_{0.6}$ probed by ^{31}P nucleus.

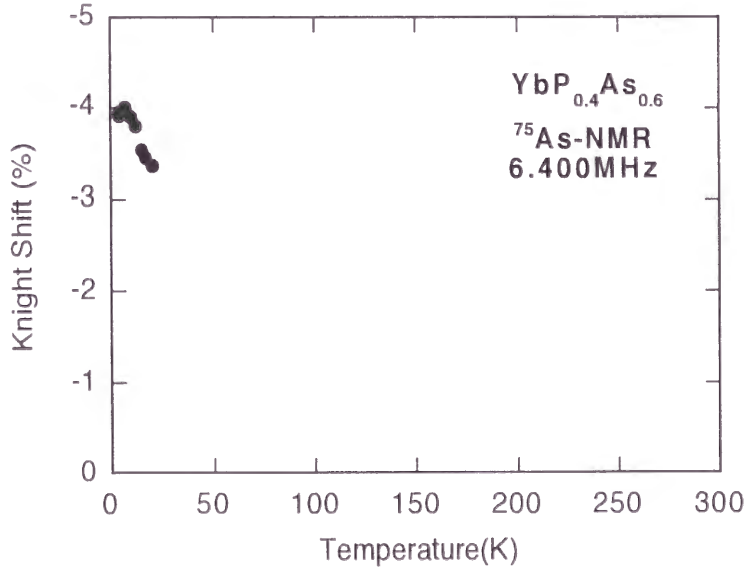

Fig. 3-6(b). Temperature dependence of the Knight Shift of $YbP_{0.4}As_{0.6}$ probed by ^{75}As nucleus.

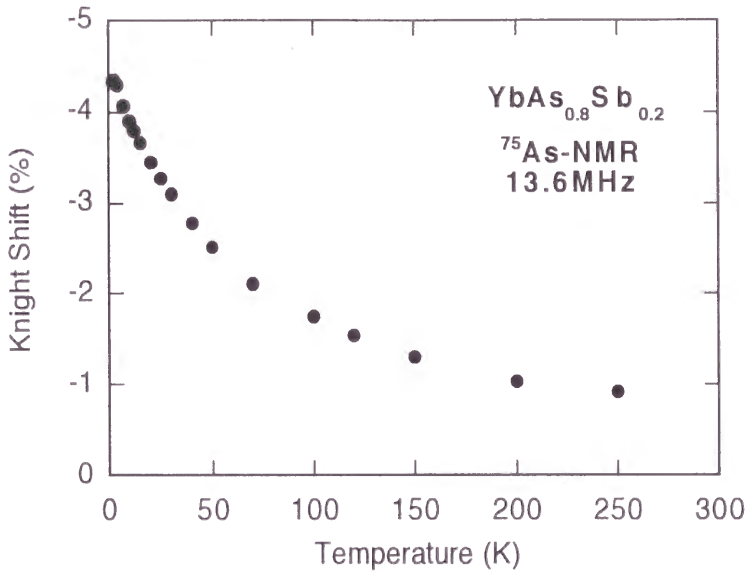

Fig. 3-7. Temperature dependence of the Knight Shift of $YbAs_{0.8}Sb_{0.2}$ probed by ^{75}As nucleus.

In Figs. 3-8, 3-9, 3-10, 3-11, 3-12(a), 3-12(b) and 3-13, we exhibit the Knight shift K(T) vs magnetic susceptibility χ plot for YbN, YbP, YbAs, YbSb, $YbP_{0.4}As_{0.6}$ probed by ^{31}P nuclei, $YbP_{0.4}As_{0.6}$ probed by ^{75}As nuclei and $YbAs_{0.8}Sb_{0.2}$ probed by ^{75}As, respectively. The data of χ for YbN, YbP, YbAs and YbSb were measured by Ott et al. The data of χ for $YbP_{0.4}As_{0.6}$ and $YbAs_{0.8}Sb_{0.2}$ were measured by us using a SQUID magnetometer. The Knight shift K(T) is expressed by χ and the hyperfine coupling constant A_{HF} as follows:

$$K(T) = \frac{A_{HF}}{N \mu_B} \chi, \qquad (3\text{-}2)$$

where N and μ_B are the Avogadro's number and the Bohr magneton, respectively. It is found that the K(T) vs χ plot does not follow a simple linear relation, but exhibits a distinct change of the slope around 70 K in all Yb-monopnictides. The nonlinearity is observed also below about 10 K. The Knight shift have week temperature dependence below 10 K, while the susceptibility still increase with decreasing temperature. The nonlinearity below about 10 K has strong sample dependence and may come from the impurity, although X-ray diffraction detected no impurity phase. Thus we will not concern this nonlinearity anymore.

The hyperfine coupling constants were estimated by using eq. (3-2) and summarized in Table 3-1 with the temperature T_{HF} where the change of the slope was observed.

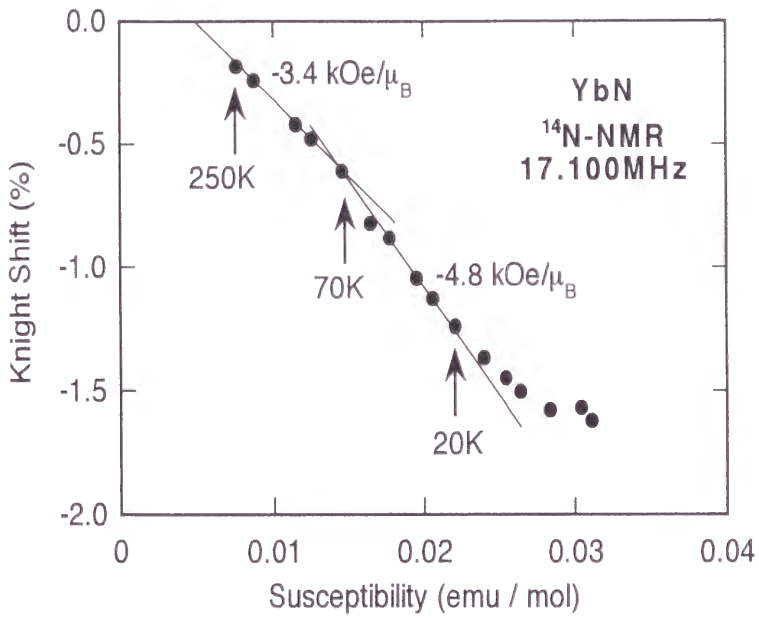

Fig. 3-8. K-χ plot of YbN.

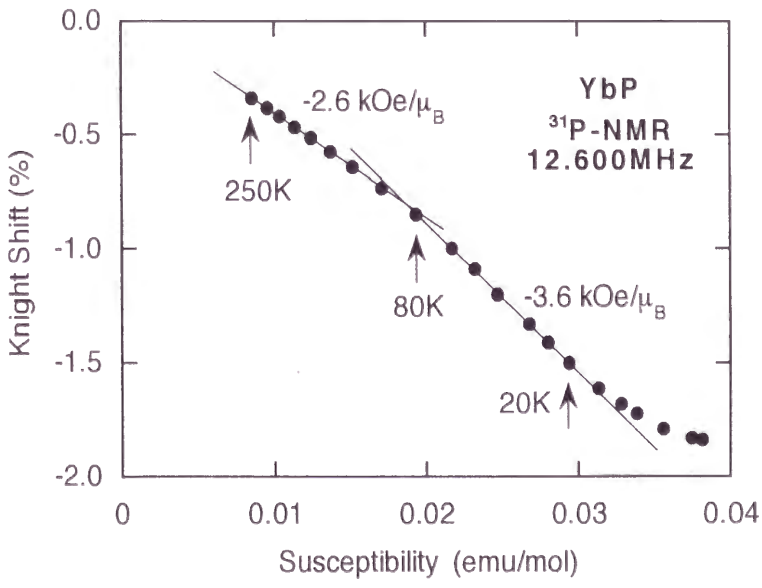

Fig. 3-9. K-χ plot of YbP.

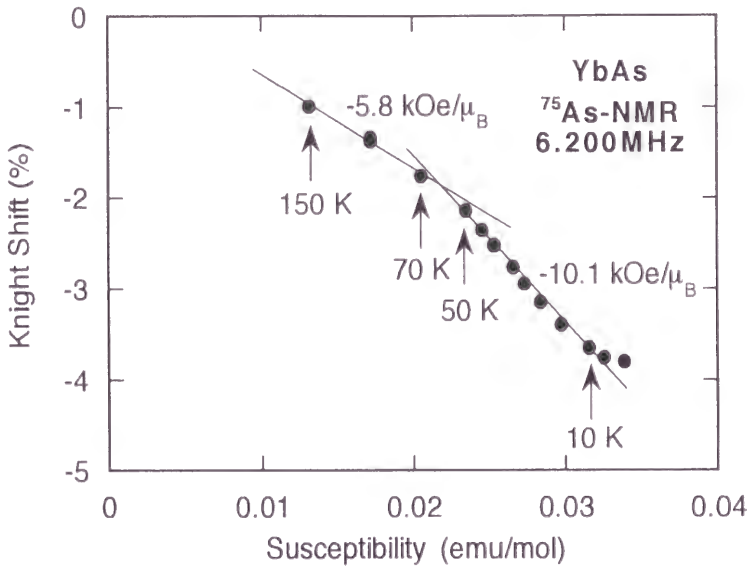

Fig. 3-10. K-χ plot of YbAs.

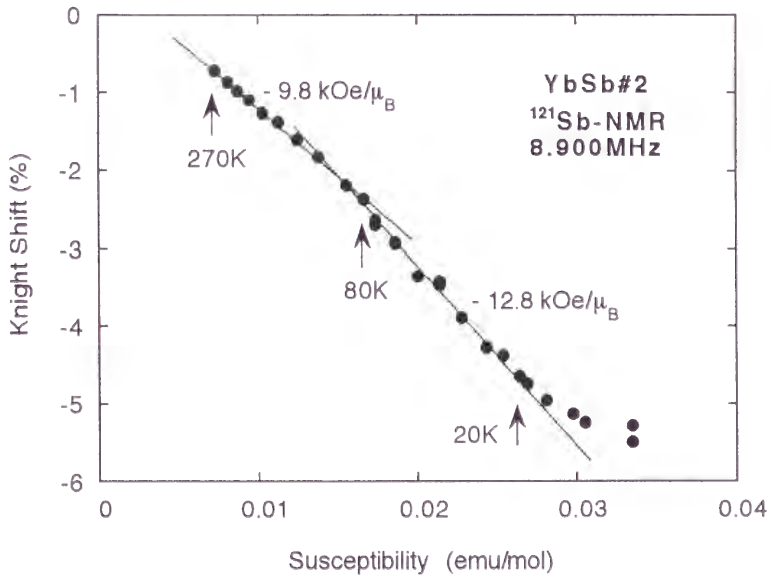

Fig. 3-11. K-χ plot of YbSb.

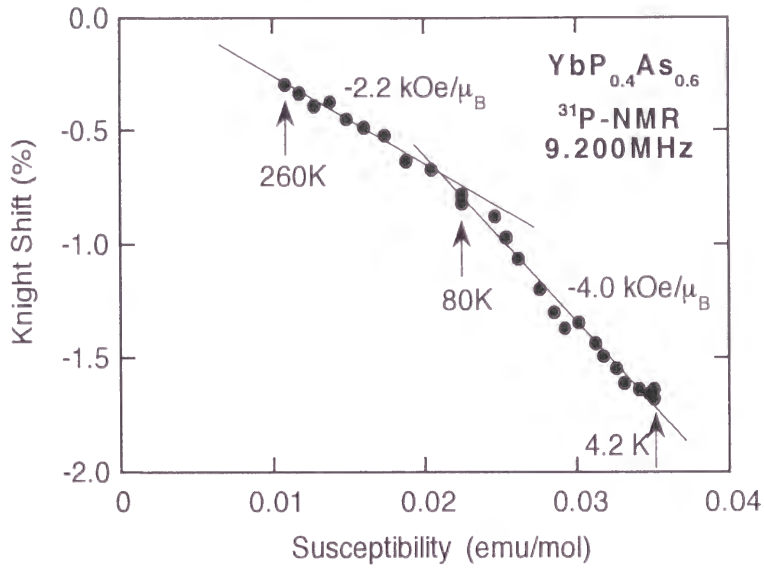

Fig. 3-12(a). K-χ plot of $YbP_{0.4}As_{0.6}$ probed by ^{31}P nucleus.

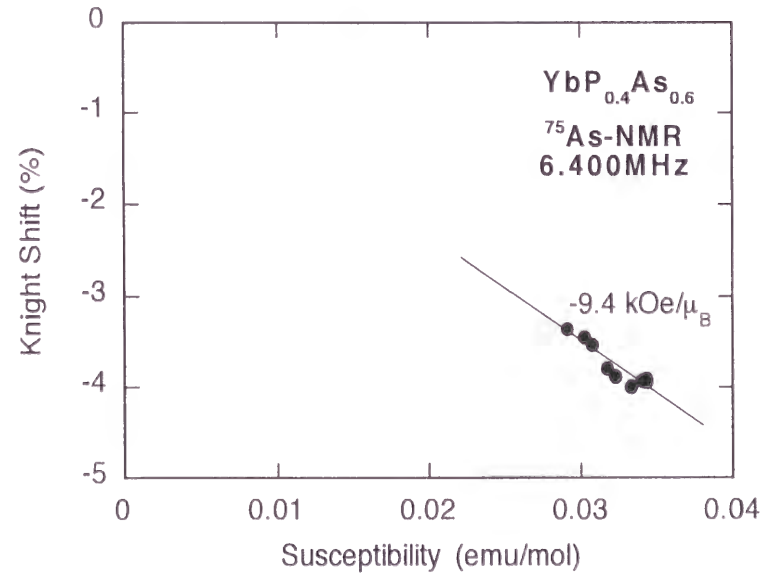

Fig. 3-12(b). K-χ plot of $YbP_{0.4}As_{0.6}$ probed by ^{75}As nucleus.

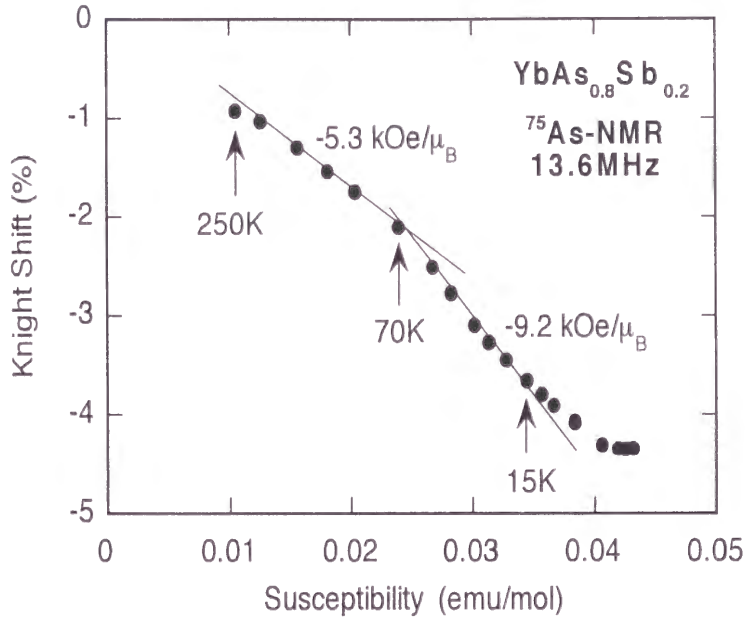

Fig. 3-13. K-χ plot of $YbAs_{0.8}Sb_{0.2}$ probed by ^{75}As nucleus.

		Hyperfine coupling constant A_{HF} (kOe/μ_B)		T_{HF} (K)
		$T < T_{HF}$	$T_{HF} < T$	
YbN	^{14}N-NMR	-4.8	-3.4	70
YbP	^{31}P-NMR	-3.6	-2.6	80
$YbP_{0.4}As_{0.6}$	^{31}P-NMR	-4.0	-2.2	80
	^{75}As-NMR	-9.4		
YbAs	^{75}As-NMR	-10.1	-5.8	60
$YbAs_{0.8}Sb_{0.2}$	^{75}As-NMR	-9.2	-5.3	70
YbSb	^{121}Sb-NMR	-12.8	-9.8	80

Table 3-1 Hyperfine coupling constants A_{HF} and the temperature T_{HF} where the change of the hyperfine coupling constant was observed.

3.1.2 Spin-lattice Relaxation Time T_1

Next, we show the temperature dependence of the spin-lattice relaxation rate $1/T_1$ above 1.5 K. The temperature dependence of the relaxation rate $1/T_1$ for YbN, YbP, YbAs, YbSb and $YbAs_{0.8}Sb_{0.2}$ are shown in Figs. 3-14, 3-15, 3-16, 3-17 and 3-18, respectively. The relaxation rate $1/T_1$ is almost temperature independent in this temperature range, indicating that the magnetic moments are well localized. In YbP and YbAs, a broad minimum of $1/T_1$ around 10 K was observed. A small peak of $1/T_1$ corresponding to the phase transition at 5 K was observed in YbSb.

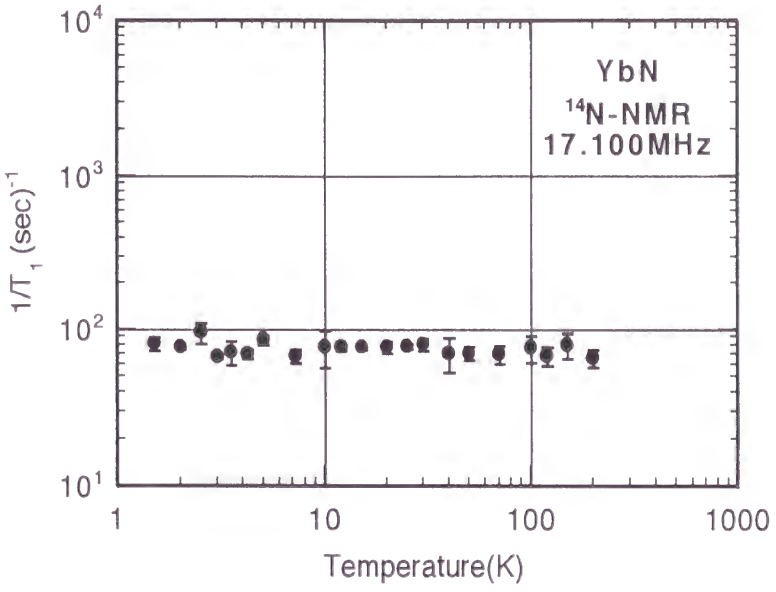

Fig. 3-14. Temperature dependence of $1/T_1$ of YbN.

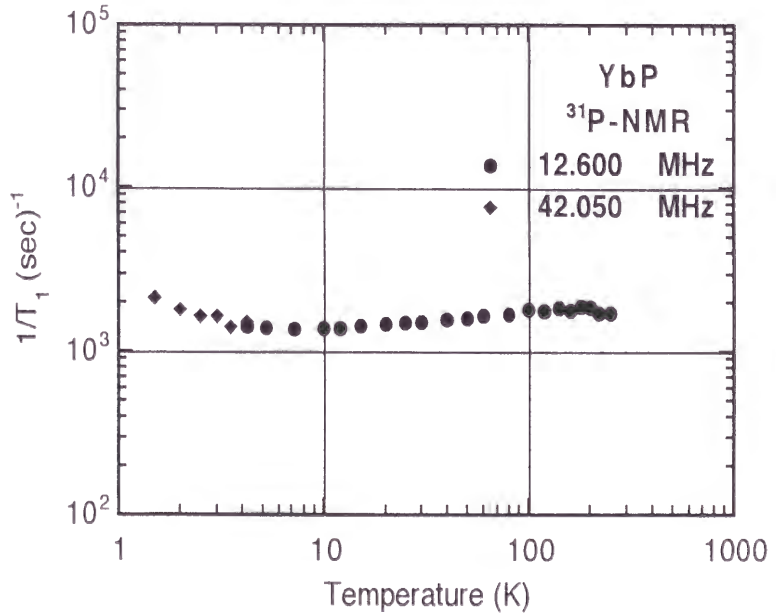

Fig. 3-15. Temperature dependence of $1/T_1$ of YbP.

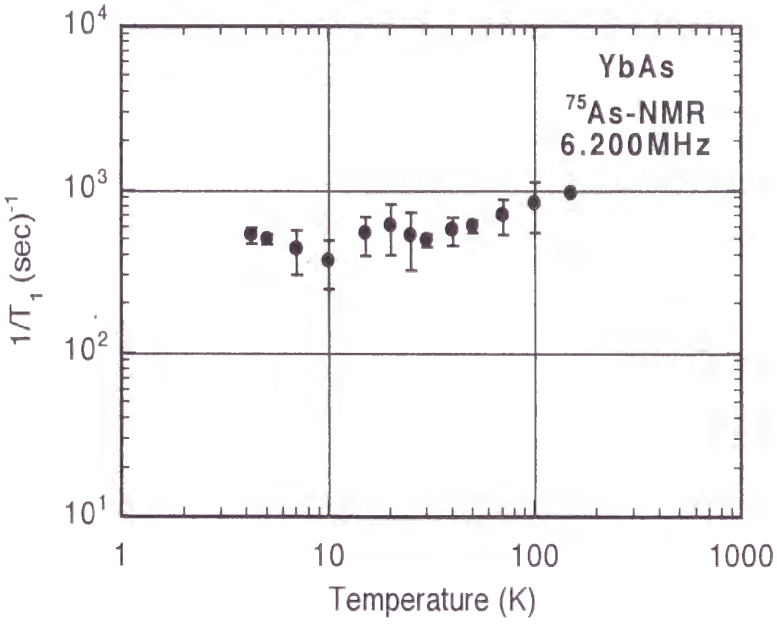

Fig. 3-16. Temperature dependence of $1/T_1$ of YbAs.

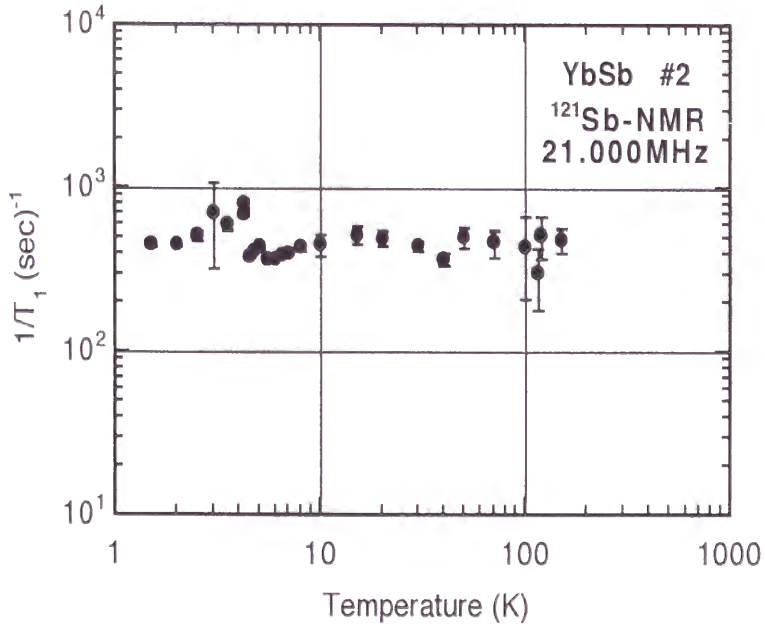

Fig. 3-17. Temperature dependence of $1/T_1$ of YbSb.

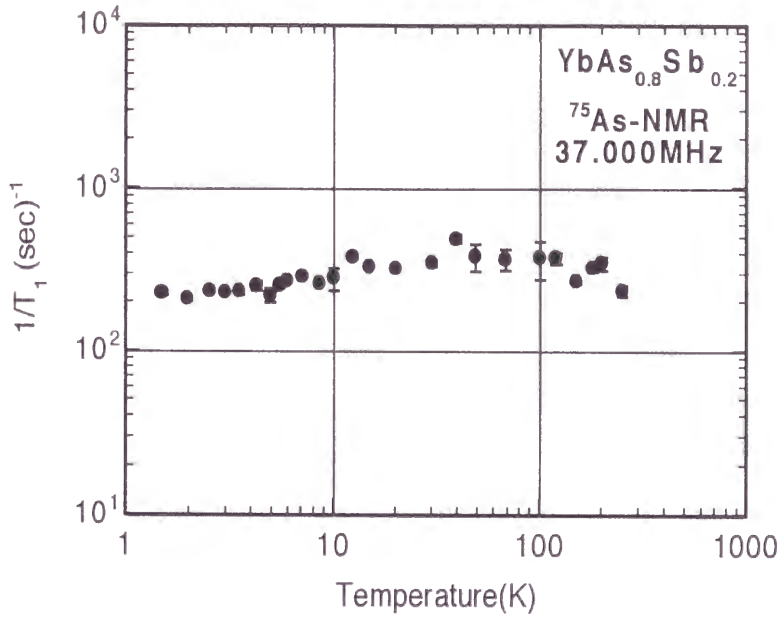

Fig. 3-18. Temperature dependence of $1/T_1$ of $YbAs_{0.8}Sb_{0.2}$ probed by ^{75}As nucleus.

3.2 *Phase Transition and Ordered State in YbAs*

In this section we present the results of YbAs below 1.5 K. Figure 3-19 shows the ^{75}As spin-echo spectra around T_N at the resonant frequency of 7.800 MHz. At 0.61 K, the NMR spectrum is almost Lorentzian-type with a half line-width at half-maximum (HWHM) of ~50 Oe, while below 0.40 K it is an extremely broad one with a HWHM of ~1.35 kOe. This extremely broad spectrum clearly shows the existence of a magnetic ordering. Between 0.40 K and 0.61 K, each NMR spectrum consists of these two components. Thus it seems that paramagnetic and antiferromagnetically ordered regions coexist in this temperature range.

We show the experimental results for the spin-lattice relaxation time T_1 in YbAs. The recovery curve of the nuclear magnetization to the thermal equilibrium value was not single exponential in the temperature range below 0.6 K. It seems that the recovery of the nuclear magnetization was affected by the spin diffusion effect below T_N. The recovery of the nuclear magnetization was also affected by the coexistence of the paramagnetic and the antiferromagnetically ordered regions in the temperature range between 0.4 K and 0.6 K. The recovery curve below 0.6 K is well explained by assuming two components for $1/T_1$, though the recovery of the nuclear magnetization was affected by the above two effect between 0.4 K and 0.6 K. We regarded the longer component as the intrinsic relaxation rate $1/T_1$. Figure 3-20 shows the temperature dependence of the spin-lattice relaxation rate $1/T_1$ measured at the center of the NMR spectrum.

The relaxation rate $1/T_1$ exhibits a small peak around 0.8 K, which is followed by a rapid decrease of three orders of magnitude with decreasing temperature down to about 0.3 K. The relaxation rate $1/T_1$ below 0.2 K shows the Fermi-liquid-like behavior given as $(T_1T)^{-1}=2.9$ $(s\ K)^{-1}$.

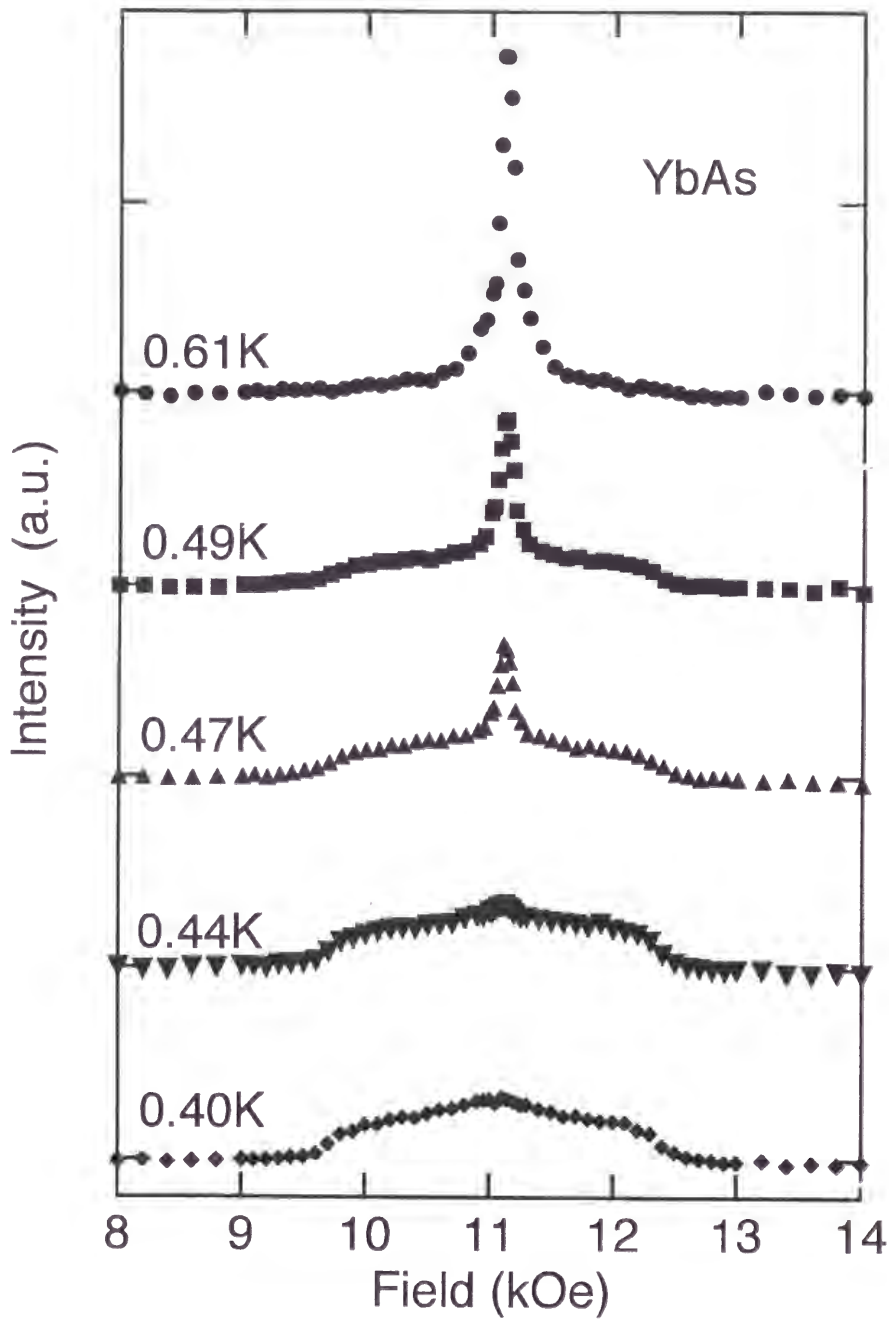

Fig. 3-19. Temperature dependence of NMR spectra of YbAs around T_N.

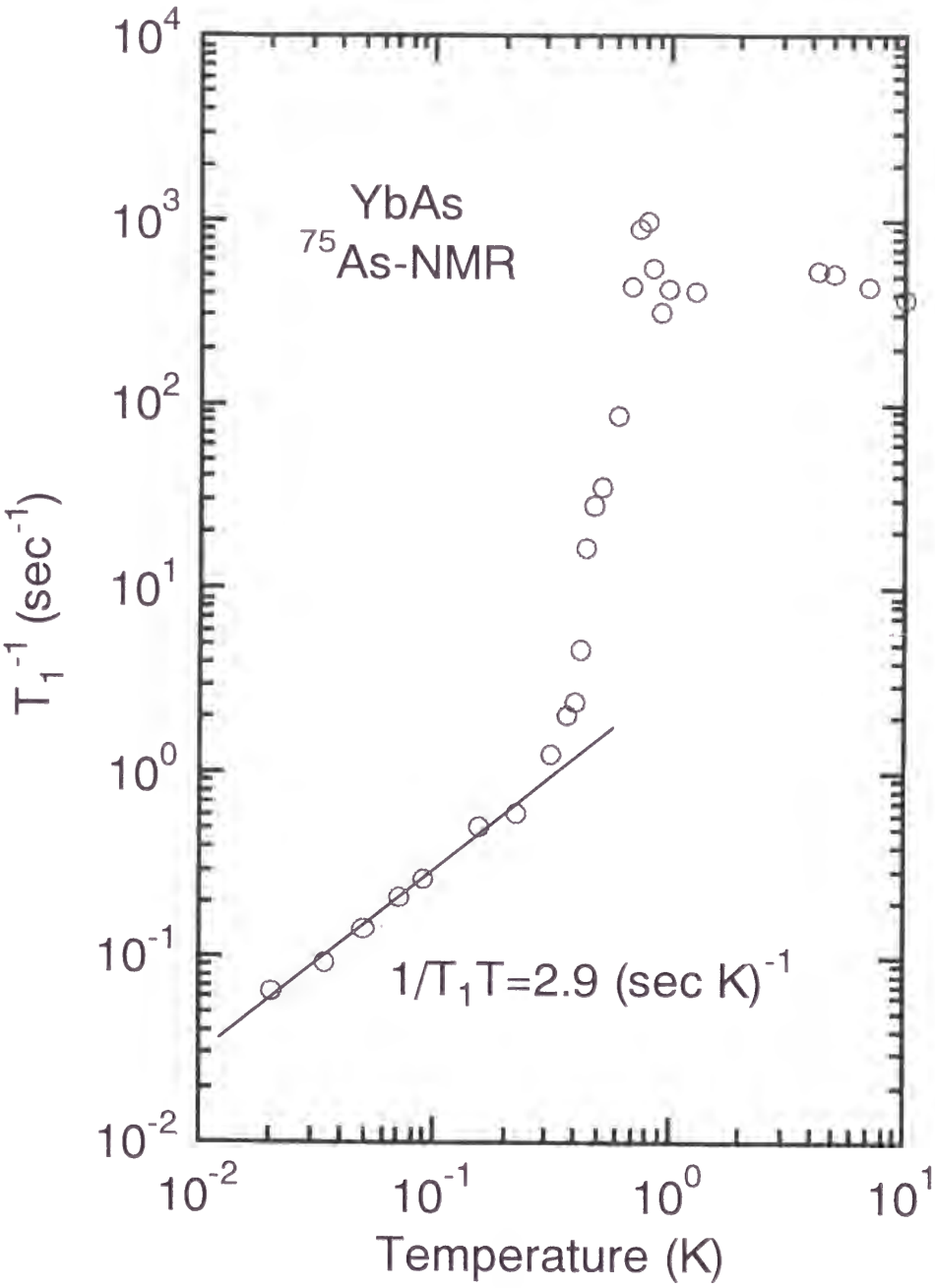

Fig. 3-20. Temperature dependence of $1/T_1$ of YbAs down to 20 mK.

3.3 Phase Transition and Ordered State in YbSb

Next, we show the experimental results concerning the phase transition in YbSb. Figures 3-21(a) and 3-21(b) show the temperature dependence of the NMR spectrum around 5 K in YbSb#1 and YbSb#2, respectively. We show the temperature dependence of the full-line width at half-maximum (FWHM) of YbSb#1 and YbSb#2 in Figs. 3-22(a) and 3-22(b), respectively. The distinct broadening of the NMR spectra at 5 K were observed in both samples of YbSb#1 and YbSb#2. Corresponding to the broadening of the NMR spectra, the spin-echo intensity decrease abruptly at 5 K as shown in Fig. 3-23. These results clearly shows the presence of a phase transition at about 5 K. NMR spectra below the transition temperature are slightly asymmetric. The FWHM below the transition temperature increases and the slope of the curve becomes steeper with decreasing temperature.

In order to clarify the character of the ordered phase in YbSb, the external magnetic field dependence of the FWHM of the NMR spectrum was measured. Figures 3-24(a) and 3-24(b) show the external magnetic field dependence of the FWHM of YbSb#1 and YbSb#2 in the ordered and the paramagnetic phases, respectively. The FWHM shows the week external magnetic field dependence in the paramagnetic phase in both samples. The FWHM of YbSb#2 at the extrapolated external magnetic field of zero is almost the same with that for LuSb, which is the nonmagnetic reference compound with no 4f holes. In the ordered phase, the FWHM is proportional to the external field with a slope steeper than that in the paramagnetic phase. The FWHM at the extrapolated external magnetic field of zero in the ordered phase is about 130 Oe larger than that in the paramagnetic phase.

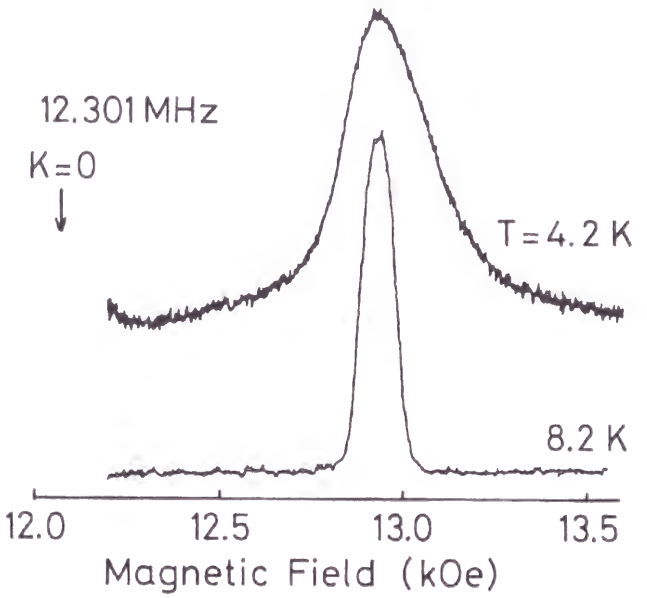

Fig. 3-21(a). NMR spectra of YbSb#1 around 5 K.

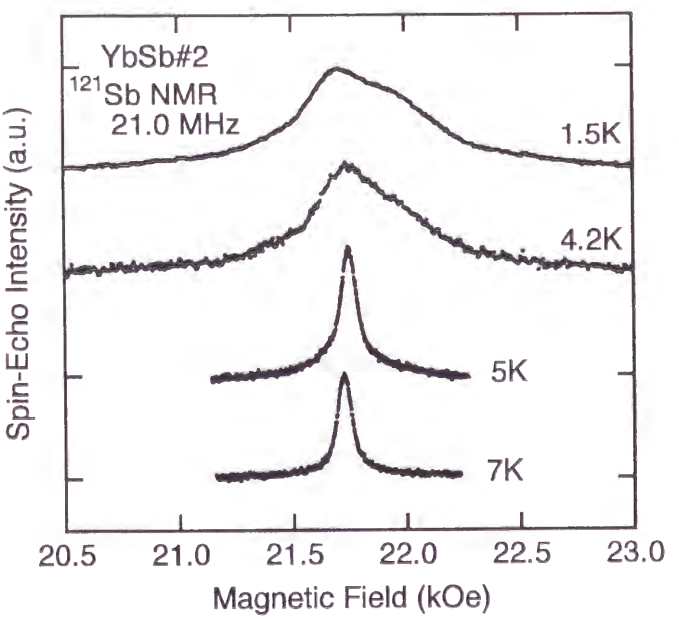

Fig. 3-21(b). NMR spectra of YbSb#2 around 5 K.

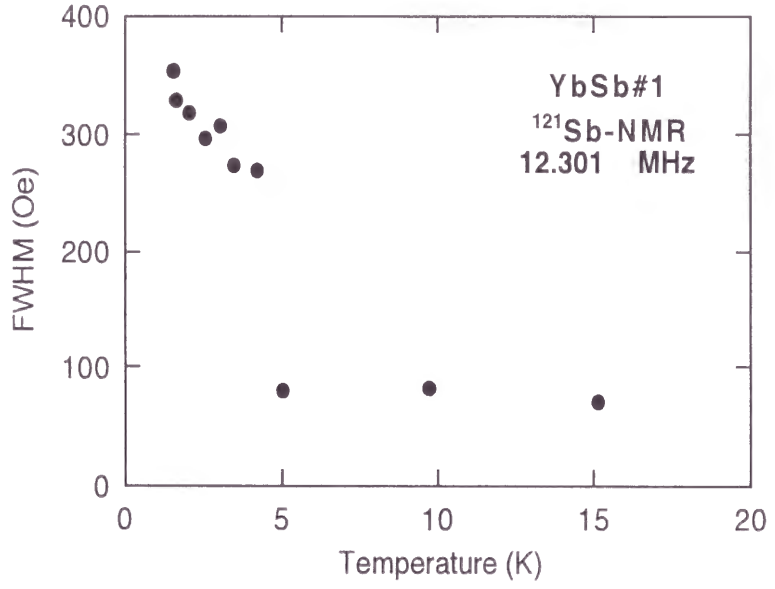

Fig. 3-22(b). Temperature dependence of FWHM of YbSb#1.

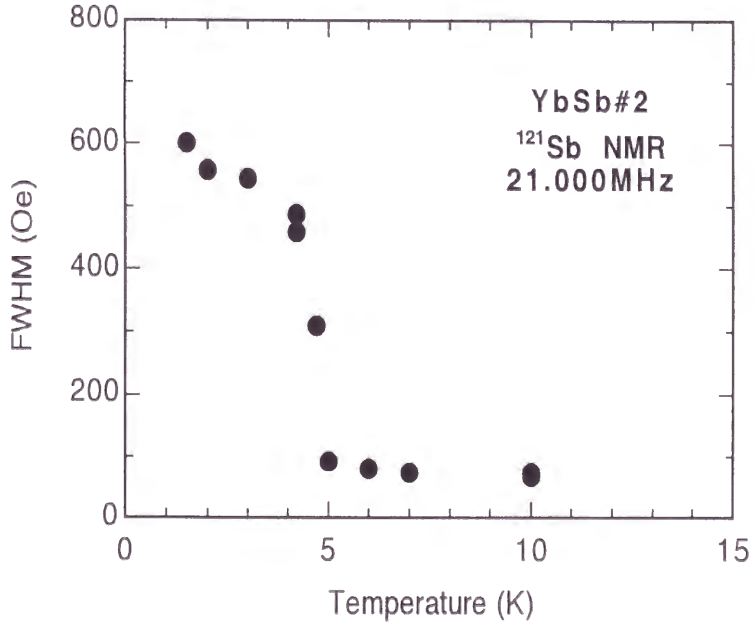

Fig. 3-22(b). Temperature dependence of FWHM of YbSb#2.

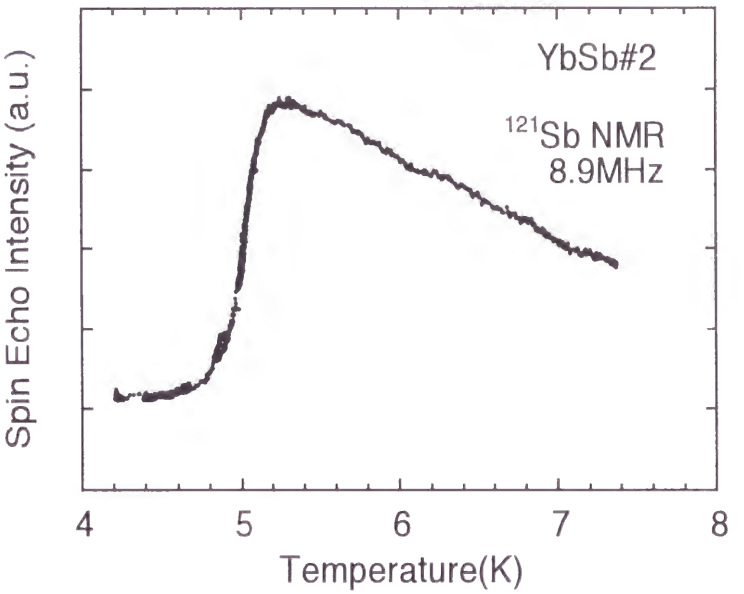

Fig. 3-23. Temperature dependence of spin-echo intensity around 5 K.

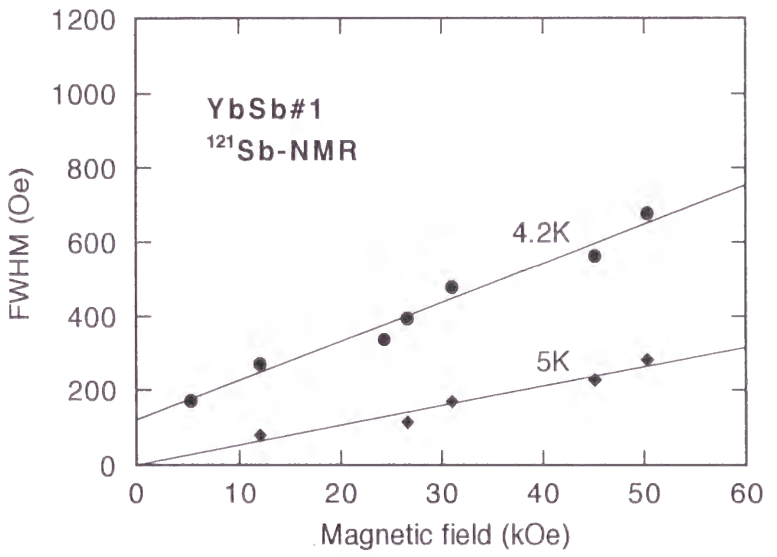

Fig. 3-24(a). External magnetic field dependence of FWHM of YbSb#1 at 4.2 K and 5 K.

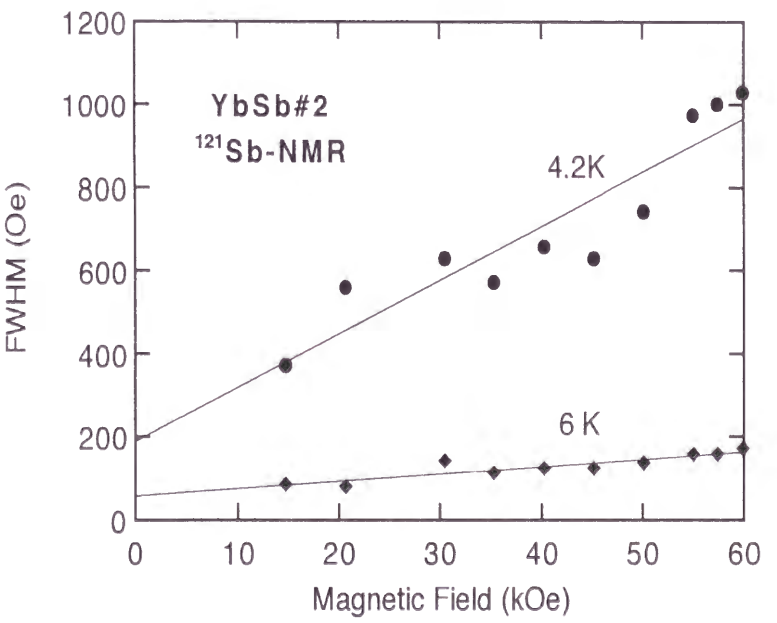

Fig. 3-24(b). External magnetic field dependence of FWHM of YbSb#2 at 4.2 K and 6 K.

Chapter 4 Analysis and Discussion

4.1 Paramagnetic States in Yb-monopnictides

4.1.1 Temperature Dependent Hyperfine Coupling Constants

First we discuss the Knight shift and the temperature-dependent hyperfine coupling constants in Yb-monopnictides. The temperature-dependent hyperfine coupling constants were observed in all Yb-monopnictides. Since we have performed NMR measurements on the ligand nucleus, the experimentally obtained hyperfine coupling constants are affected by both the hybridization of the f-electrons with ligand electrons and the intra-atomic interaction. The mechanism of the hyperfine coupling is not clear in Yb-monopnictides, though the importance of the p-f mixing for the hybridization of the f-electrons with ligand electrons was discussed for YbP.[4-1] As can be seen in Table 3-1 the temperatures T_{HF} where the hyperfine coupling constants change are almost the same in all Yb-monopnictides, although the magnitude of the CEF splittings in YbN are about two times larger than those in YbSb. Thus it is difficult to account the temperature-dependent hyperfine coupling constants by the p-f mixing model. Here it is interesting to investigate the pnictogen dependence of the hybridization of the f-electrons with ligand electrons. The intra-atomic hyperfine coupling constants have been calculated for the outer 3s, 4s and 5s electrons in P, As and Sb atoms, respectively.[4-2] We summarize the experimental and calculated ratios of hyperfine coupling constants in Table 4-1 by using the values of the hyperfine coupling constants $^{31}A_{HF}$, $^{75}A_{HF}$ and $^{121}A_{HF}$ for YbP, YbAs and YbSb, respectively, for the experimental values. It is found that the experimental values of $^{75}A_{HF}/^{31}A_{HF}$ and $^{121}A_{HF}/^{31}A_{HF}$ above and below T_{HF} are close to those of the calculated values, respectively. The values of the Knight shifts for $YbP_{0.4}As_{0.6}$ measured at the ^{31}P and ^{75}As sites are almost the same with those for YbP and YbAs, respectively. This indicates that there is no pnictogen dependence of the hybridization of the f-electrons with ligand electrons. Thus it is found that the Knight shift for Yb-monopnictides are primarily due to the intra-atomic interaction of the polarization of outer s electrons in the ligand atoms, though there must be the hybridization of the f-electrons with ligand electrons. These results are similar to the case of Ce-monopnictides.[4-3] However, the origin of the temperature dependent hyperfine coupling is not clear. Below about the same temperature of 70 K, neutron scattering experiments show the anomalies in Yb monopnictides: (1) the anomalous splitting of the Γ_8 CEF first excited states.[4-4, 4-5, 4-6]

(2) the cross-over from the Lorentzian-typed spectrum to the Gaussian-typed one in the quasi-elastic neutron scattering experiments.[4-7] The difference of the hyperfine coupling constants above and below about 70 K is possibly related to these anomalies observed by neutron scattering experiments.

	$^{75}A_{HF}/^{31}A_{HF}$	$^{121}A_{HF}/^{31}A_{HF}$
$T > T_{HF}$	2.2	3.8
$T_{HF} > T$	2.8	3.6
Calculated value	2.5	3.6

Table 4-1 The ratios of the hyperfine coupling constants in Yb-monopnictides and the calculated values.

4.1.2 *Temperature Dependence of Spin Fluctuation Rate*

Next we discuss the spin-lattice relaxation rate $1/T_1$ in the paramagnetic state. In general the relaxation rate $1/T_1$ can be expressed in terms of the dynamical susceptibility $\chi(q,\omega)$ as follows,[4-1]

$$\frac{1}{T_1} = 2\gamma_N^2 k_B T \sum_q A_q A_{-q} \lim_{\omega \to 0} \frac{\mathrm{Im}\,\chi(q,\omega)}{\omega} \frac{1}{N\mu_B^2}, \qquad (4\text{-}1)$$

where γ_N is the nuclear gyromagnetic ratio of the probe nucleus, A_q is the spatial Fourier transform of the hyperfine coupling constant. The relaxation rate in this temperature range is mainly dominated by the fluctuation of 4f moments. To estimate the fluctuation rate of Yb 4f magnetic moments $1/\tau_f$ from the results for the relaxation rate $1/T_1$, we here assume that the fluctuation spectrum of Yb 4f moments is Lorentzian and the fluctuation rate of the 4f moments $1/\tau_f$ has no q-dependence. Then the imaginary part of the dynamical susceptibility is given as

$$\mathrm{Im}\,\chi(q,\omega) = \chi(q) \frac{\omega/\tau_f}{(1/\tau_f)^2 + \omega^2} \qquad (4\text{-}2)$$

Further, it is assumed that $\chi(q)$ has no q-dependence and is given as the static susceptibility per mole χ_0. It is noted that the inelastic neutron scattering experiment showed that short-range spin correlations begin to develop below about 20 K.[4-8] Thus, it is proper to assume that $1/\tau_f$ and $\chi(q)$ have no q-dependence above 20 K. Then, we get the following expression,

$$\frac{1}{T_1} = 2\gamma_N^2 k_B T \left[\sum_i A_{THF}(R_i)^2 + \sum_i \frac{2\mu_B^2}{r_i^6} \right] \frac{\chi_0 \tau_f}{N\mu_B^2}, \qquad (4\text{-}3)$$

where A_{THF} is the transferred hyperfine coupling constant and the second term of the square brackets is the dipolar contribution, which is calculated over 100×100×100 unit

cells to be 12.04×10^6, 4.99×10^6, 4.25×10^6, 4.11×10^6 and 2.86×10^6 $(Oe/\mu_B)^2$ for YbN, YbP, YbAs, $YbAs_{0.8}Sb_{0.2}$ and YbSb, respectively. Here, it should be noted that the dipole interaction contributes to $1/T_1$, while it does not contribute to the Knight shift in the cubic symmetry of magnetic ions. It is further assumed to estimate τ_f quantitatively that only the nearest-neighbor Yb 4f moments contribute to the transferred hyperfine coupling. Thus, the first term of the square brackets is replaced by $z_0(A_{HF}/z_0)^2$, where z_0 (=6) is the number of the nearest-neighbor Yb ions, and A_{HF} is the hyperfine coupling constant deduced from the K(T) vs χ plot. We use the lower temperature values of the transferred hyperfine coupling constant. We show the temperature dependence of the fluctuation rate $1/\tau_f$ below 50 K deduced by the above mentioned procedure for YbN, YbP, YbAs, $YbAs_{0.8}Sb_{0.2}$ and YbSb in Fig. 4-1.

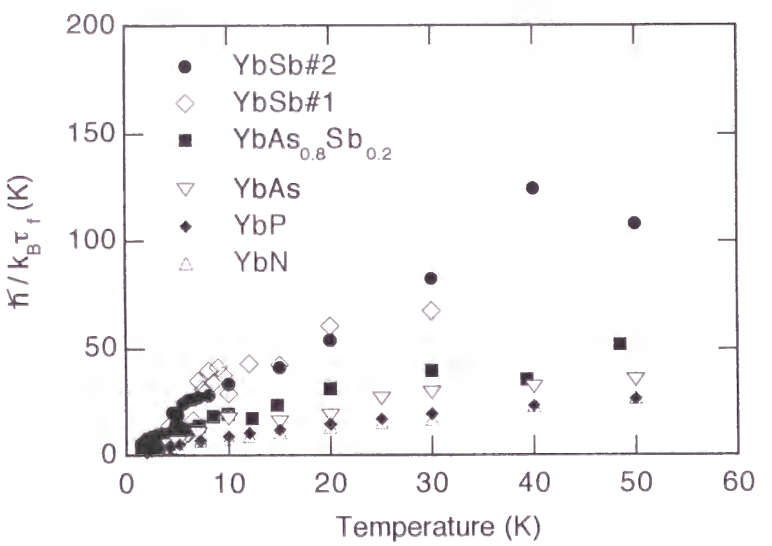

Fig. 4-1. Temperature dependence of the spin fluctuation rate for Yb-monopnictides.

There are two remarkable points in Fig. 4-1: (1) in all Yb-monopnictides, the fluctuation rate $1/\tau_f$ decreases with $\sqrt{T}$ dependence and approaches to zero as temperature decreases; (2) the values of $1/\tau_f$ become large as the pnictogen changes from As to Sb, though the rate $1/\tau_f$ are almost the same quantitatively among YbN, YbP and YbAs. Below we discuss the temperature and the pnictogen dependence of the fluctuation rate $1/\tau_f$.

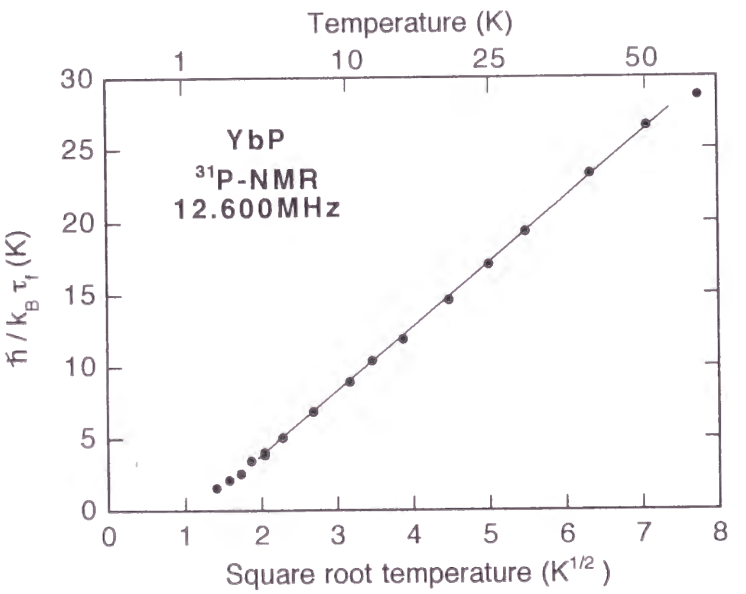

Fig. 4-2. Temperature dependence of the spin fluctuation rate for YbP. Solid line shows square root temperature dependence.

Firstly, we discuss the temperature dependence of the fluctuation rate $1/\tau_f$. The $\sqrt{T}$ dependence of the rate $1/\tau_f$ is confirmed by plotting the rate $1/\tau_f$ vs square root temperature as in Fig. 4-2. In all Yb-monopnictides, the rate $1/\tau_f$ show the $\sqrt{T}$ dependence as many other heavy Fermion compounds.[4-9, 4-10, 4-11] This behavior is theoretically discussed by the calculation based on the degenerate Anderson model using 1/N expansion, where N is the degree of orbital degeneracy for the 4f states.[4-12] On this model the localized 4f electron spin fluctuates through the mixing with conduction

electrons. The $\sqrt{T}$ dependence of $1/\tau_f$ in Yb-monopnictides suggests that the dynamical properties in Yb-monopnictides can be explained by the degenerate Anderson model as in other heavy Fermion compounds. On the other hand, the fluctuation rate $1/\tau_f$ shown in Fig. 4-1 can be compared with a half width Γ of the fluctuation spectrum measured by quasi-elastic neutron scattering experiments.[4-7] The temperature dependence of $1/\tau_f$ is consistent with the results of quasi-elastic neutron scattering experiments above 20 K. However, there is a difference between the fluctuation rate $1/\tau_f$ and the half width Γ below about 20 K: the rate $1/\tau_f$ continues to decrease with decreasing temperature, while the half width Γ approaches to a finite value.[4-7] This difference can be attributed to the failure of the assumption that the fluctuation rate $1/\tau_f$ and $\chi(q)$ are q-independent. Indeed the development of the short-range spin correlations up to 20 K which is observed by inelastic neutron scattering experiments indicates the presence of the q-dependence of $\chi(q,\omega)$.

Next, we concern the pnictogen dependence of the fluctuation rate $1/\tau_f$. As mentioned above, the values of $1/\tau_f$ are almost the same among YbN, YbP and YbAs, though the values of spin-lattice relaxation time, gyromagnetic ratios and hyperfine coupling constants are different each other in these compounds, respectively. This is consistent with the fact that these compounds have similar physical properties: broad peaks in specific heat around 5 K, Néel temperatures. On the other hand, the values of $1/\tau_f$ become large as the pnictogen changes from As to Sb. This is also consistent with the fact that YbSb is an exceptional case in Yb-monopnictides: only YbSb does not show distinct magnetic ordering and physical properties of YbSb does not obey the systematic change in Yb-monopnictides.[4-13] Therefore, both the similarities in the physical properties of YbN, YbP and YbAs and the anomalous behavior in YbSb are confirmed by this NMR measurements in terms of dynamical aspect.

4.2 *Phase Transition and Fermi Liquid Like Behavior in YbAs*

4.2.1 *Phase Transition*

In this subsection we discuss the properties of the ordered state and the phase transition in YbAs from both a static and a dynamical point of view.

The NMR spectrum below 0.40 K is an extremely broad one with a HWHM of ~1.35 kOe and almost temperature independent. This extremely broad spectrum clearly shows the existence of a magnetic ordering. In the presence of the ordered magnetic moment, the effective local magnetic field at a nuclear site is the vector sum of the external magnetic field H_{ext} and the internal magnetic field H_A. This broad spectrum cannot be explained by simple antiferromagnetically ordered moment of which the direction distributes randomly in the powdered sample,[4-14] because this broad spectrum has a peak at its center. It is unlikely that this peak originates from the paramagnetic region because the width of this peak is about 10 times larger than that of the narrower component of the spectrum above 0.40 K. This broad spectrum including a peak can be explained by the model that the ordered magnetic moment partially orients its direction perpendicular to H_{ext}. There are two probable mechanisms for the orientation of the magnetic moment perpendicular to H_{ext}. The first mechanism is the domain motion in a single crystal as observed by the neutron diffraction experiments under external magnetic field up to 6 T.[4-15] The second mechanism is a rotation of particles of sample so as to orient the magnetic moment perpendicular to H_{ext}. The magnitude of H_{ext} in this study is as low as about 1 T. Then, not all of the direction of the particles of sample must orient perpendicular to H_{ext}. It is not clear that the orientation of magnetic moment originates from either or both of the above mechanisms. So we tentatively suppose that the partial orientation of magnetic moment perpendicular to H_{ext} is expressed by one Gaussian function with width Δ. Then, the number of the nuclei dN of which the direction of H_A is between θ and $\theta+d\theta$ to the direction of H_{ext} is given by

$$dN \propto \left[A + B \exp\left\{ -\frac{(\theta - \pi/2)^2}{\Delta^2} \right\} \right] \sin\theta \, d\theta, \qquad (4\text{-}4)$$

where the first term of square brackets comes from randomly distributed moment[4-14] and the second term is due to partially oriented magnetic moment perpendicular to H_A. As

we have measured the NMR spectrum at a fixed resonance frequency, a resonant magnetic field H_0 is given as a function of H_{ext} as follows,

$$H_0^2 = H_{ext}^2 + H_A^2 + 2\,H_{ext}\,H_A \cos\theta, \qquad (4\text{-}5)$$

where θ is the angle between H_A and H_{ext}. From the derivative of eq.(4-5) by θ and eq.(4-4), we get the number of the nuclei $|dN/dH_{ext}|$ of which the effective field is equal to H_0 as a function of H_{ext}. The internal magnetic field H_A, the constants A and B and the orientation width Δ are obtained by fitting the experimental spectra. Figure 4-3 shows the NMR spectrum at 0.32 K with the fitting curve calculated by the above procedure using the values of H_A=1.35 kOe, A/B=1 and Δ=0.075 π rad. The fitting curve which is convoluted by a Lorentzian function with a HWHM of 150 Oe is also shown in Fig. 4-3.

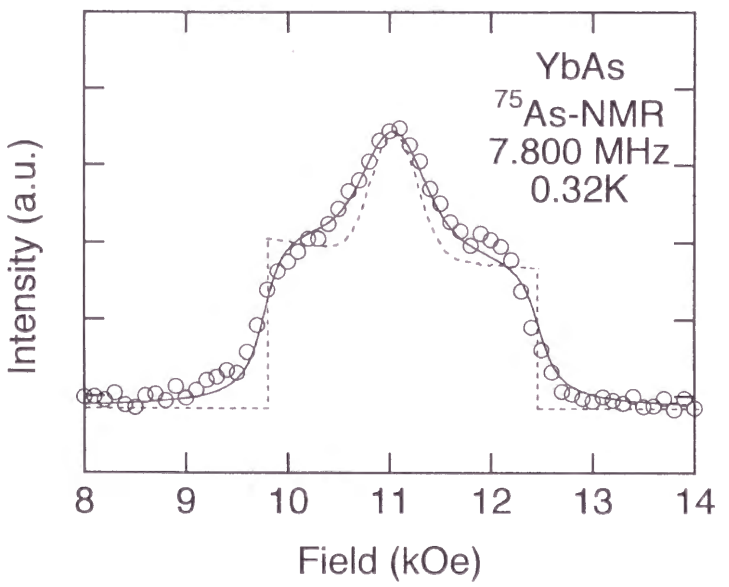

Fig. 4-3. An NMR spectrum of YbAs in the ordered state (open circle). The dashed and solid lines show the fitting curves before and after the convolution, respectively.

The magnitude of the antiferromagnetically ordered moment is estimated to be 0.61 μ_B from the value of H_A of 1.35 kOe and the calculated dipole field of 2.20 kOe/μ_B. Here, it should be noted that if the transferred hyperfine interaction is isotropic, the transferred hyperfine field is canceled out each other at As sites in the NaCl-type crystal structure due to their symmetry of the magnetic structure of type III . The magnitude of the ordered moment is consistent with that of 0.6 μ_B[4-15] and 0.86 μ_B[4-16] determined by neutron diffraction measurements. The previous Mössbauer-spectroscopy measurements also showed that the direction of the magnetic moment is almost perpendicular to H_{ext}.[4-17]

The NMR spectrum between 0.40 K and 0.61 K seems to consist of two components as is shown in Fig. 3-19. The presence of such two components in this temperature region indicates that the paramagnetic and the antiferromagnetically ordered regions coexist. The broader component of the spectrum is fitted by the same procedure which used in the fitting of the spectrum below 0.40 K. Figure 4-4 shows the temperature dependence of the magnitude of H_A. The temperature dependence of the relative proportion of the ordered region to the whole of the sample is obtained from the ratios of areas of the paramagnetic and ordered components in the spectrum as also shown in Fig. 4-4.

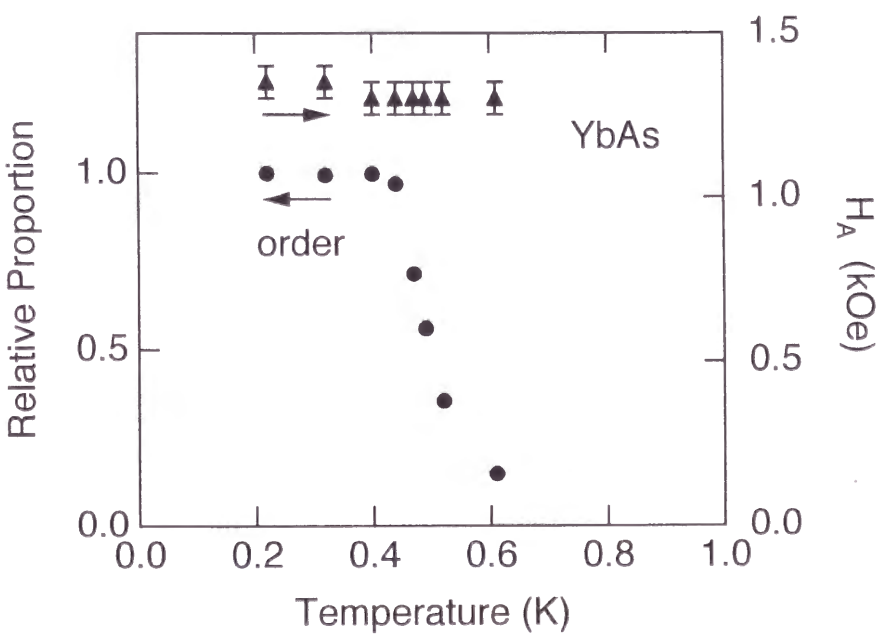

Fig. 4-4. Temperature dependence of the relative proportion of ordered state (solid circle) and the internal field H_A (solid triangle).

By the above analysis, it becomes clear that the paramagnetic and the antiferromagnetically ordered regions coexist in the temperature range between 0.40 K and 0.61 K. Further, in this temperature range, the internal magnetic field H_A is almost temperature independent, though the relative proportion of the ordered region increases with decreasing temperature. This means that the phase transition in YbAs is first order. However, no hysteresis was observed which is characteristic of a first order transition. This can be interrupted as follows: the lattice defects and/or inhomogeneities of the sample give rise to a distribution of transition temperatures in the sample and overshadow the hysteretic behavior. These results are quite consistent with those obtained from neutron-diffraction and Mössbauer-spectroscopy. In neutron-diffraction measurements[4-15, 4-16], an unusual tail in the temperature dependence of the staggered magnetization was observed as shown in Fig. 4-5.

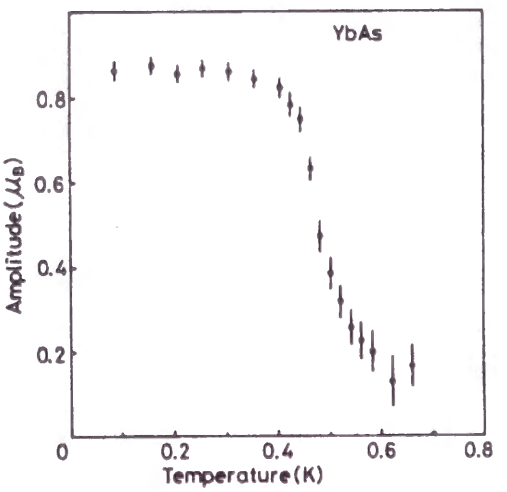

Fig. 4-5. Temperature dependence of the staggered magnetization measured by neutron diffraction.[4-15]

Further, in ^{170}Yb Mössbauer-spectroscopy measurements,[4-17] the similar behavior of the Mössbauer spectrum with that of NMR was observed. Figure 4-6 shows the Mössbauer spectrum of YbAs around T_N. In the temperature range well below T_N, the Mössbauer spectrum has the magnetic hyperfine structure (Zeeman quintet). On the other hand, it is a single paramagnetic line well above T_N. At the temperature near the phase transition, the Mössbauer spectrum is the superposition of the above mentioned two spectra. The temperature dependence of the Yb^{3+} hyperfine field, which remains constant below T_N was obtained from these Mössbauer spectra as shown in Fig. 4-7(a). Figure 4-7(b) shows the temperature dependence of the relative proportion of the ordered region. Our results are quite consistent with the results obtained by these Mössbauer-spectroscopy measurements. Therefore, it seems that the magnetic transition in YbAs is first order. However, the relaxation rate $1/T_1$ shows a small peak around 0.8 K. The origin of this small peak remains unclear for the moment.

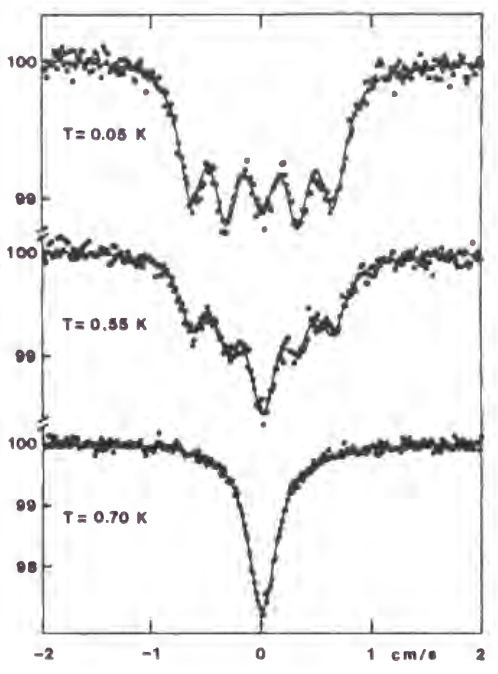

Fig. 4-6 Temperature dependence of Mössbauer spectra.[4-17]

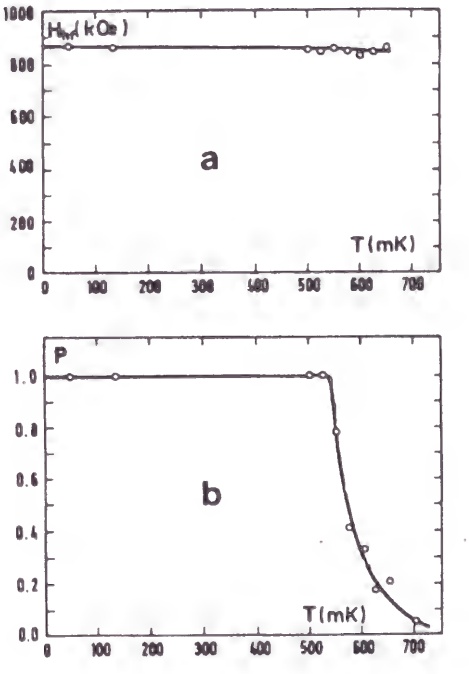

Fig. 4-7 Temperature dependence of
(a) the Yb^{3+} hyperfine field,
(b) the relative proportion of the ordered region.[4-17]

The relaxation rate $1/T_1$ below 0.8 K exhibits a rapid decrease of three orders of magnitude with decreasing temperature down to 0.3 K. This rapid decrease of $1/T_1$ seems to be due to the scattering of spin waves. The temperature dependence of $1/T_1$ for the two-magnon, or Raman process for $k_BT<<E_g$ in antiferromagnet is expressed by

$$\frac{1}{T_1} \propto T^2 \exp(-\frac{E_g}{k_B T}), \qquad (4\text{-}6)$$

where E_g is an energy gap.[4-18] The relaxation rate in the temperature range between 0.3 K and 0.8 K can be well fitted by eq. (4-6) with E_g=3.6 K as shown in Fig. 4-8. Two spin wave excitations with energy gaps were observed by neutron scattering experiments.[4-19] One spin wave branch has a constant excitation energy of 3.6 K, whereas the other has a strong dispersion with an energy gap of 0.93 K. The magnitude of the energy gap is the same with that of the dispersionless spin wave excitation observed by neutron scattering experiments. On the other hand, the temperature dependence of $1/T_1$ below 0.2 K cannot be explained by the scattering of the spin waves. Instead it is explained by the Korringa process as mentioned in the next subsection.

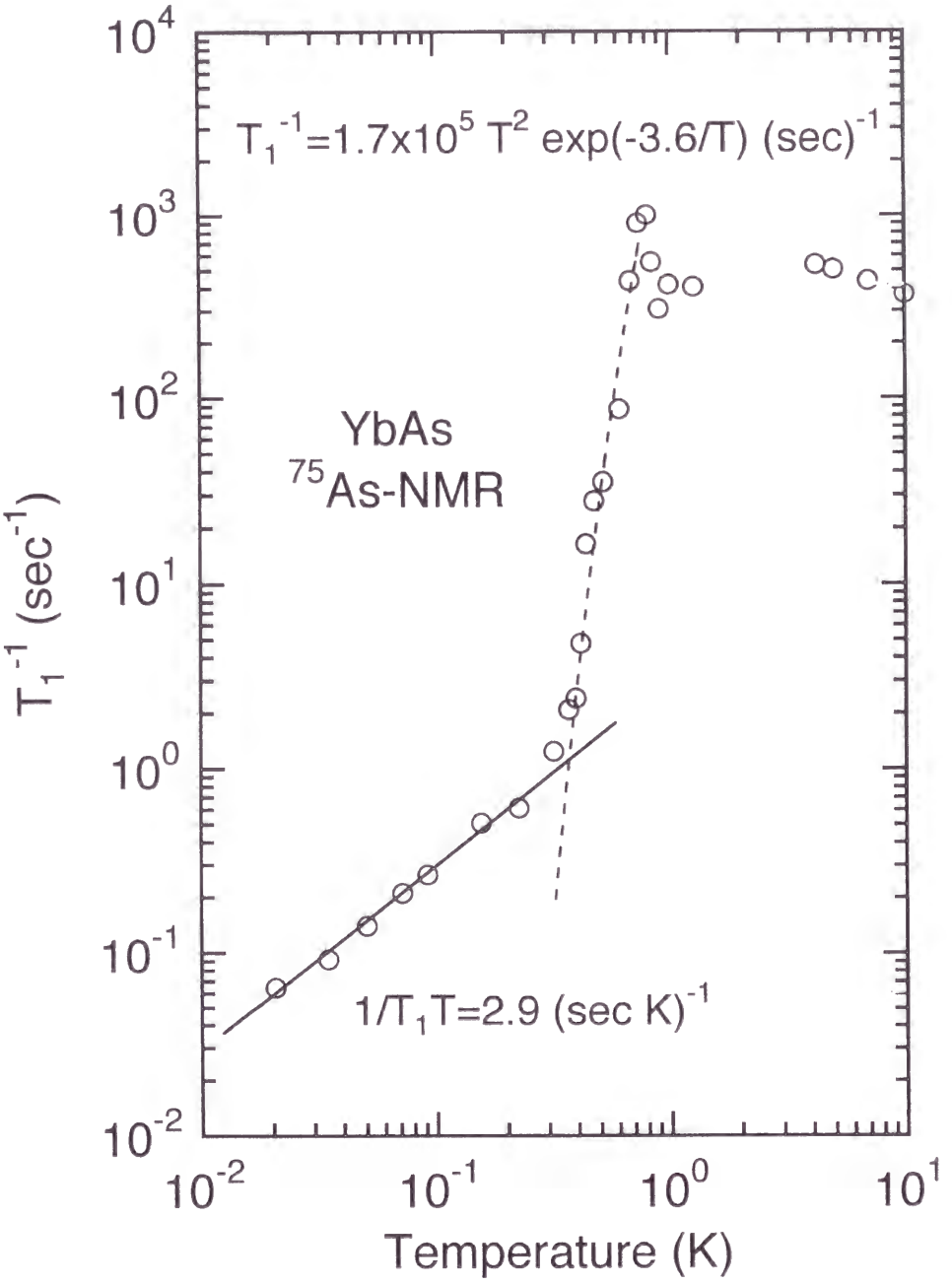

Fig. 4-8. Temperature dependence of $1/T_1$ for YbAs down to 20 mK. The dashed line indicates the temperature dependence of $1/T_1$ due to the two magnon process with an energy gap of 3.6 K. The solid line indicates the Korringa relation with $(T_1T)^{-1}=2.9\ (s\ K)^{-1}$.

4.2.2 *Fermi Liquid Like Behavior*

Next, we discuss the Fermi-liquid-like behavior in YbAs. The relaxation rate below 0.2 K follows the Korringa relation with $(T_1T)^{-1}=2.9$ (s K)$^{-1}$. The spin-lattice relaxation rate $1/T_1$ follows the Korringa relation given as $(T_1T)^{-1}$=constant when the nuclear energy relaxes to conduction electrons. We have measured the temperature dependence of $1/T_1$ for ^{75}As in the non-magnetic reference compound LuAs which has no 4f-holes to examine the effect of the 4f-holes in YbAs. The relaxation rate $1/T_1$ for LuAs follows the Korringa relation with $(T_1T)^{-1}=0.03$ (s K)$^{-1}$. Now it becomes clear that the value of $(T_1T)^{-1}$ for YbAs is about 100 times larger than that for LuAs. This clearly shows that there is a large enhancement of the number of low energy excitation due to the 4f-holes.

For a single rare-earth impurity obeying the Hund's rule in a simple metal, Kuramoto and Müller-Hartmann proved that the Korringa relation holds well below the Kondo temperature.[4-20] We discuss our results on the basis of this theory. The relation between the ω-linear part of Im $\chi(q,\omega)$ and the static susceptibility χ_{4f} was obtained at absolute zero temperature as follows:

$$\lim_{\omega\to 0}\frac{\mathrm{Im}\,\chi(q,\omega)}{\omega}=\frac{\pi\hbar\chi_{4f}^2}{k_B N C}, \qquad (4\text{-}7)$$

where N is the orbital degeneracy of 4f moment and C is the Curie constant. This relation is considered to be valid as long as a single impurity is considered. Then, using the Knight shift K and the nuclear gyromagnetic ratio γ_N, we get the Korringa constant from eqs. (3-2), (4-1) and (4-7) as follows,

$$\frac{1}{T_1 T K^2}=\frac{2\pi\hbar\gamma_N^2}{N C}. \qquad (4\text{-}8)$$

For YbAs, using the experimentally obtained values of $(T_1T)^{-1}=2.9$ (s K)$^{-1}$ and K=-3.8 %, we get $(T_1TK^2)^{-1}=2.0\times10^3$ (s K)$^{-1}$. This value is by one order of magnitude smaller than the right-hand side value of eq. (4-8) of 6.3×10^4 (s K)$^{-1}$, which is obtained by using the values for the CEF ground state of N=2 and C=$(1.33\ \mu_B)^2/k_B$. The theory

which treats the effects of periodic f-electrons and the magnetic order is highly desired to explain the difference between the experimental and theoretical values of $(T_1TK^2)^{-1}$ for YbAs.

Here, it is interesting to compare the experimentally obtained value of $(T_1TK^2)^{-1}$ for YbAs with those for other heavy Fermion compounds. Equation (4-8) is reduced to

$$\frac{N\,C}{T_1\,T\,K^2\,\gamma_N^2} = 2\pi\,\hbar. \qquad (4\text{-}9)$$

Because the value of the right-hand side of eq. (4-9) contains no parameter, the value of the left-hand side of eq. (4-9) (from now on, referred to as MKC) should be the same value for all heavy Fermion compounds as long as the spin fluctuations could be described in the framework of the single impurity model. Figure 4-9 shows the values of MKC multiplied by k_B/μ_B^2 for many heavy Fermion compounds, in which the Fermi-liquid-like relation given as $(T_1T)^{-1}$=constant was observed. In calculating the value of MKC, the values of the degeneracy N and the Curie constant C for free Yb^{3+} or Ce^{3+} ions are used for $YbAl_2$[4-21, 4-22], $YbAl_3$[4-21, 4-22] and $CeSi_x$[4-23, 4-24] system. For the other compounds, the values of N and C for the CEF ground state are used.

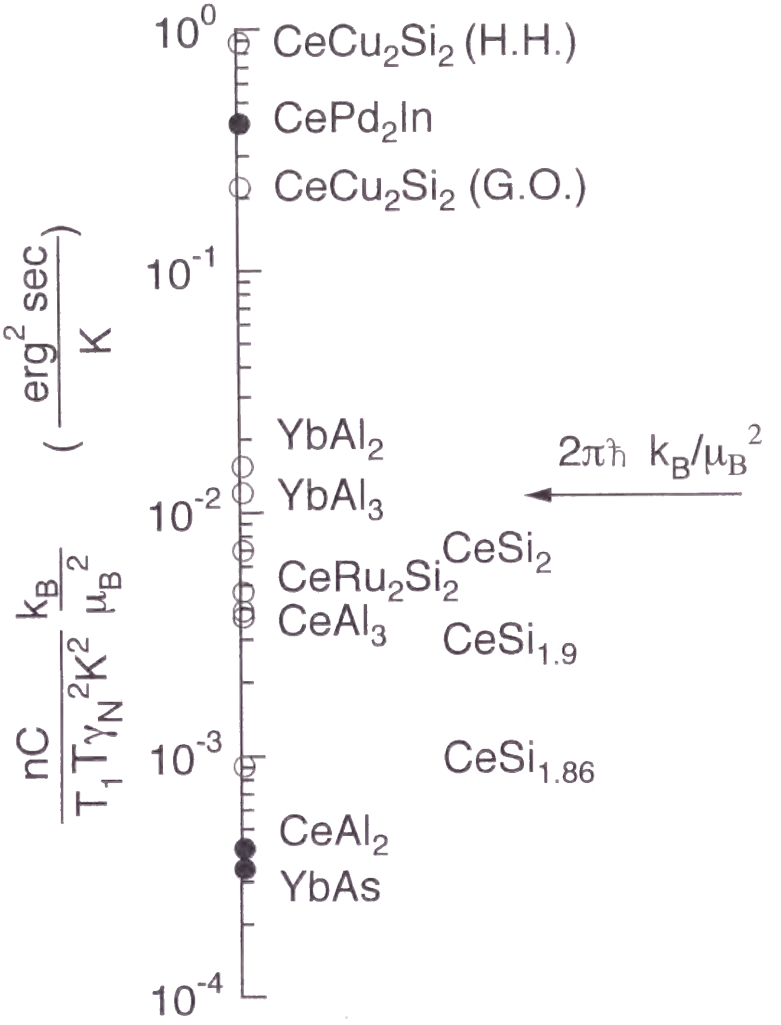

Fig. 4-9. The modified Korringa constants (MKC, see text) for many heavy Fermion compounds. Open and solid circles indicate the compounds with non-magnetic and magnetically ordered ground state, respectively. The arrow indicates the theoretical values of $2\pi\hbar\ k_B/\mu_B^2$. The points of $CeCu_2Si_2$ marked (H.H.) and (G.O.) represent, respectively, the calculated values using the CEF ground state reported by Horn et al. and by Goremychkin and Osborn.

In Fig. 4-9, we can find a tendency as follows. The values of MKC for the compounds with non-magnetic ground state such as $YbAl_2$, $YbAl_3$, $CeRu_2Si_2$[4-25, 4-26], $CeSi_2$ and $CeAl_3$[4-27, 4-28, 4-29, 4-30] are near the theoretical value. The deviation of the values of MKC from the theoretical value is considered to be the inherent difference in the dynamical behavior between the single impurity and the periodic 4f ion systems. Indeed, from the calculation performed by using the slave-boson approach to the periodic Anderson model, it was reported that the theoretical value of $(T_1T)^{-1}$ in the periodic system differs by a factor of the Curie constant C multiplied by k_B/μ_B^2 from the single impurity model.[4-31] This slave-boson calculation accounts for the value of $(T_1T)^{-1}$ in $CeRu_2Si_2$.

On the other hand, the values of MKC for $CeAl_2$[4-32, 4-33, 4-34, 4-35] and YbAs with magnetically ordered ground state are much smaller than the theoretical value. The values of MKC for $CeAl_2$ and YbAs are almost the same, though the values of $(T_1T)^{-1}$, γ_N and the Curie constant C are different in the two compounds, respectively. The value of MKC for $CeSi_x$ system becomes small and approaches to the values of MKC for $CeAl_2$ and YbAs with decreasing x from the value of 2 to 1.86. The $CeSi_x$ system with $x<1.80$ exhibits a ferromagnetic phase transition.[4-23] This indicates that the value of MKC becomes small with the system approaching to the magnetic transition. Thus it seems that the value of MKC is reduced by a magnetic order. The reduction of the value of $(T_1T)^{-1}$ in the magnetically ordered state compared to that in the paramagnetic state was observed in other heavy Fermion compounds such as URu_2Si_2[4-36], $CePd_2In$[4-37] and UPd_2Al_3[4-38]. Unfortunately we cannot obtain the values of MKC for URu_2Si_2, UPd_2Al_3 and the paramagnetic state in $CePd_2In$, because some of the values of the Curie constant, the degeneracy and the Knight shift for these compounds are not available. So the values of MKC for these compounds do not appear in Fig. 4-9.

However, the values of MKC for $CeCu_2Si_2$[4-39, 4-40, 4-41] and the ordered state in $CePd_2In$[4-37] deviate from the above mentioned tendency. For $CeCu_2Si_2$, two different CEF level schemes were proposed by Horn et al.[4-42] and by Goremychkin and Osborn[4-43] from inelastic-neutron-scattering measurements. The values of MKC for both CEF ground states were plotted in Fig. 4-9 and exhibit large deviations from the theoretical value. The origin of this deviation might be associated with the non-Fermi-liquid behavior. The Fermi-liquid-like relation $(T_1T)^{-1}$=constant in $CeCu_2Si_2$ was observed just above the superconducting transition temperature T_c, where the non-Fermi-

liquid behavior typically given as the -T ln T dependence of the specific heat was observed.[4-44] For $CePd_2In$, there is no appropriate explanation for the large deviation in the Korringa relation. However, the large value of $(T_1T)^{-1}$ in non-magnetic reference compound $LaPd_2In$ with no 4f electron may be related with this large deviation.[4-37]

From these results, the value of MKC for YbAs can be explained by the above mentioned tendency for heavy Fermion compounds. This means that the relaxation rate for YbAs below 0.2 K is dominated by the Korringa process just like in other heavy Fermion compounds. Therefore, it is found that the large enhancement of the number of excitation in YbAs originates from the large density of states at Fermi level. However, the question why the heavy Fermion state can be realized in the low carrier concentration system remains. For this question, it has been pointed out that the localized spins mutually quench their spins by the antiferromagnetic correlations between the localized spins. The Kondo type screening of the localized spins by conduction electron spins just help the mutual quenching of the localized spins to make the whole system a singlet.[4-45] By this mechanism it seems that the heavy Fermion state can be realized in the low carrier concentration compounds such as YbAs.

4.3 Phase Transition in YbSb around 5 K

In this section, we discuss anomalous properties in YbSb around 5 K. As shown in section 3.3, our NMR measurements on YbSb#1 and YbSb#2 clearly show the presence of a phase transition at about 5 K, though neutron diffraction measurements did not detect any phase transition down to 7 mK.[4-46] Below, we discuss the magnetic properties of the ordered state in YbSb.

First, we discuss the external magnetic field dependence of FWHM. The FWHM in the ordered state depends on the external magnetic field stronger than that in the paramagnetic state. There is little difference between the magnitude of the susceptibility at the temperature of 4.2 K and 6 K. Thus, the difference in the magnitude of the FWHM at 4.2 K and 6 K cannot be explained by the difference of the susceptibility. It seems that a new mechanism arises for the FWHM in the ordered state. Now, we recall the fact that the external magnetic field can induce antiferromagnetically ordered moments in the presence of antiferroquadrupolar ordering.[4-47] Indeed, previous Mössbauer spectroscopy measurements showed that antiferromagnetic moments are induced in the presence of the external magnetic field.[4-48] Thus, it seems that antiferroquadrupolar ordering is realized in the ordered state. However, the CEF ground-state Γ_6 doublet has no quadrupole moment. For this discrepancy, from the theoretical point of view, the magnetic polaron model was proposed.[4-49] On this model, the first excited Γ_8 quartet, which has quadrupole moment, is placed energetically very close to the ground state. This may related to the anomalous splitting of CEF excitations between 4f-Γ_6 and 4f-Γ_8 in inelastic neutron scattering experiments.[4-4]

Next, we discuss the additional broadening of the NMR spectrum at the extrapolated magnetic field of zero in the ordered phase. The specific heat measurements[4-50] and Mössbauer spectroscopy experiments[4-48] detected a phase transition around 5K without external magnetic field. Thus, it seems that there is an additional broadening of the NMR spectrum under zero field, though the external magnetic field dependence of the FWHM is not measured under external magnetic field below about 5 kOe. An antiferromagnetic order broadens an NMR spectrum, if hyperfine fields at the nucleus are not canceled each other by their symmetry. We suppose that the additional broadening of the NMR spectrum at the extrapolated field of zero comes from the ordered magnetic moment. If a magnetic structure is known, the magnitude of the

ordered magnetic moment can be estimated from the magnitude of the FWHM. However, the magnetic structure of YbSb is unknown because neutron diffraction experiments did not detect any long-range magnetic ordering. Thus, it is necessary to suppose a magnetic structure of YbSb to estimate the magnitude of the ordered moment. From the previous neutron diffraction measurements, it is reported that YbN and YbAs have a magnetic structure of type III with ordering wave vector k=[1 0 1/2] and YbP has a structure of type II with k=[1/2 1/2 1/2].[4-46] In YbP with a type II structure, both the transferred hyperfine field and the dipole field at P nucleus are entirely canceled. It was reported that the additional broadening of the NMR spectrum below the Néel temperature is as small as about 10 Oe in YbP.[4-1] The magnitude of this additional broadening is one tenth of that in YbSb. Thus, we assume that YbSb has the magnetic structure of type III. Here, it should be noted that the hyperfine field is considered to be a sum of the transferred hyperfine field and the dipole field. However, the transferred hyperfine field induced by the magnetic moment with type III structure is entirely canceled at Sb site in the NaCl-type crystal structure. Thus, the ordered magnetic moment makes the hyperfine field at Sb site only through the dipole-dipole interaction. The magnetic moment of Yb ion m_l at site l with a ordering wave vector k is given as follows:

$$m_l = A_k \cos(k R_l + \phi_k) u_k , \qquad (4\text{-}10)$$

where A_k is the amplitude of the sine wave modulation, ϕ_k is the phase factor, R_l is the position of the magnetic moment and u_k is a unit vector along the direction of the magnetic moment. By the analogy with the results of the previous neutron diffraction[4-15] and Mössbauer spectroscopy[4-17] studies in YbAs, the following are assumed: the magnetic moments are arrayed perpendicular to the c-axis; the phase factor is $\pi/4$ corresponding to a (++--) sequence. Using the above mentioned assumption and k=[1 0 1/2], the hyperfine field at Sb site is calculated over 100×100×100 unit cells to be 1.825 kOe/μ_B. Therefore, the magnitude of the FWHM at the extrapolated external magnetic field of zero (130 Oe) is corresponding to the hyperfine field induced by the magnetic moment of about 0.07 μ_B. The ordering of this extremely reduced moment can explain the discrepancy between the Mössbauer spectroscopy measurements[4-48] and the neutron

diffraction experiments[4-46] at 5 K. The neutron diffraction experiments exclude the existence of only the antiferromagnetic ordering with magnetic moment larger than 0.1 μ_B. Therefore, our NMR measurements explain both the neutron diffraction and the Mössbauer effect measurements consistently. The existence of the phase transition around 5 K in the different samples indicates that this transition is intrinsic not due to impurity effects, though its nature remains unclear.

References

(4-1) S. Takagi, A. Oyamada and T. Kasuya: J. Phys. Soc. Jpn. 57 (1988) 1456.

(4-2) R. E. Watson and L. H. Bennett: Phys. Rev. B 15 (1977) 502.

(4-3) K. Hiraoka, Y. Kasamatsu, K. Kojima and T. Hihara: Physica B 186-188 (1993) 535.

(4-4) A. Dönni, A. Furrer, P. Fischer, F. Hulliger and P. Wachter: Physica B 171 (1991) 353.

(4-5) K. Ohoyama, M. Kohgi, T. Nakane, M. Arai, A. D. Taylor, A. Oyamada and T. Suzuki: Physica B 180&181 (1992) 250.

(4-6) L. Keller, W. Henggeler and A. Furrer: Europhys. Lett. 26 (1994) 353.

(4-7) K. Ohoyama, M. Kohgi, T. Otomo, T. Osakabe, A. Oyamada and T. Suzuki: Physica B 186-188 (1993) 451.

(4-8) K. Ohoyama, T. Osakabe, A. Dönni, M. Kohgi, A. Oyamada and T. Suzuki: Physica B 213&214 (1995) 119.

(4-9) A. Qachaou, E. Beaurepaire, M. Benakki, B. Lemius, J. P. Kappler, A. J. P. Meyer and P. Panissod: J. Magn. Magn. Mater. 63&64 (1987) 635.

(4-10) M. Benakki, A. Qachaou and P. Panissod: J. Magn. Magn. Mater. 73 (1988) 141.

(4-11) P. Panissod, M. Benakki and A. Qachaou: J. Phys. Colloq. 49 (1988) C8-685.

(4-12) D. L. Cox, N. E. Bickers and J. W. Wilkins: J. Appl. Phys. 57 (1985) 3166.

(4-13) D. X. Li, A. Oyamada, K. Hashi, Y. Haga, T. Matsumura, H. Shida, T. Suzuki, T. Kasuya, A. Dönni and F.Hulliger: J. Magn. Magn. Mater. 140-144 (1995) 1169

(4-14) Y. Yamada and A. Sakata: J. Phys. Soc. Jpn. 55 (1986) 1751.

(4-15) A. Oyamada, P. Burlet, L. P. Regnault, A. Bouvet, R. Calemczuk, J. Rossat-Mignod, T. Suzuki and T. Kasuya: J. Magn. Magn. Mater. 90&91 (1990) 441.

(4-16) A. Dönni, P. Fischer, A. Furrer and F. Hulliger: Solid State Commun. 71 (1989) 365.

(4-17) P. Bonville, J. A. Hodges, F. Hulliger, P. Imbert, G. Jéhanno, J. B. Marimon da Cunha and H. R. Ott: Hyperfine Interactions 40 (1988) 381.

(4-18) D. Beeman and P. Pincus: Phys. Rev. 166 (1968) 359.

(4-19) A. Dönni, A. Furrer, P. Fischer, F. Hulliger and S. M. Hayden: J. Phys. Condens. Matter. 4 (1992) 4283.

(4-20) Y. Kuramoto and E. Müller-Hartmann: J. Magn. Magn. Mater. 52 (1985) 122.

(4-21) T. Shimizu, M. Takigawa, H. Yasuoka and J. H. Wernick: J. Magn. Magn. Mater. 52 (1985) 187.

(4-22) E. E. Havinga, K. H. J. Buschow and H. J. van Daal: Solid State Commun. 13 (1973) 621.

(4-23) H. Yashima, H. Mori, T. Satoh and K. Kohn: Solid State Commun. 43 (1982) 193.

(4-24) Y. Kohori, K. Asayama, T. Kohara, N. Sato, H. Yashima, H. Mori and T. Satoh: J. Magn. Magn. Mater. 52 (1985) 349.

(4-25) Y. Kitaoka, H. Arimoto, Y. Kohori and K. Asayama: J. Phys. Soc. Jpn. 54 (1985) 3236.

(4-26) P. Haen, J. Flouquet, F. Lapierre, P. Lejay and G. Remenyi: J. Low. Temp. Phys. 67 (1987) 391.

(4-27) J. L. Gavilano, J. Hunziker and H. R. Ott: Physica B 194-196 (1994) 195.

(4-28) K. Andres, J. E. Graebner and H. R. Ott: Phys. Rev. Lett. 35 (1975) 1779.

(4-29) M. J. Lysak and D. E. MacLaughlin: Phys. Rev. B 31 (1985) 6963.

(4-30) P. A. Alekseev, I. P. Sadikov, I. A. Markova, E. M. Savitskii, V. F. Terekhova and O. D. Chistyakov: Sov. Phys. Solid State 18 (1976) 1466.

(4-31) S. M. M. Evans and B. Coqblin: Phys. Rev. B 43 (1991) 12790.

(4-32) C. D. Bredl, F. Steglich and K. D. Schotte: Z. Phys. B 29 (1978) 327.

(4-33) M. Loewenhaupt and F. Steglich: Physica 86-88B (1977) 187.

(4-34) D. E. MacLaughlin, O. Peña and M. Lysak: Phys. Rev. B 23 (1981) 1039.

(4-35) J. L. Gavilano, J. Hunziker, O. Hudak, T. Sleator, F. Hulliger and H. R. Ott: Phys. Rev. B 47 (1993) 3438.

(4-36) T. Kohara, Y. Kohori, K. Asayama, Y. Kitaoka, M. B. Maple and M. S. Torikachvili: Solid State Commun. 59 (1986) 603.

(4-37) P. Vonlanthen, J. L. Gavilano, B. Ambrosini, D. Heisenberg, F. Hulliger and H. R. Ott: Z. Phys. B 102 (1997) 347.

(4-38) Y. Kitaoka, H. Tou, G. -q. Zheng, K. Ishida, K. Asayama, T. C. Kobayashi, A. Kohda, N. Takeshita, K. Amaya, Y. Ōnuki, G. Geibel, C.

Schank and F. Steglich: Physica B 206&207 (1995) 55.

(4-39) T. Ohama, H. Yasuoka, D. Mandrus, Z. Fisk and J. L. Smith: J. Phys. Soc. Jpn. 64 (1995) 2628.

(4-40) F. Steglich, J. Aarts, C. D. Bredl, W. Lieke, D. Meschede, W. Franz and H. Schäfer: Phys. Rev. Lett. 43 (1979) 1892.

(4-41) Y. Kitaoka, K. Ueda, K. Fujiwara, H. Arimoto, H. Iida and K. Asayama: J. Phys. Soc. Jpn. 55 (1986) 723.

(4-42) S. Horn, E. Holland-Moritz, M. Loewenhaupt, F. Steglich, H. Scheuer, A. Benoit and J. Flouquet: Phys. Rev. B 23 (1981) 3171.

(4-43) E. A. Goremychkin and R. Osborn: Phys. Rev. B 47 (1993) 14280.

(4-44) J. G. Sereni, C. Geibel, M. G-Berisso, P. Hellmann, O. Trovarelli and F. Steglich: Physica B 230-232 (1997) 580.

(4-45) K. Ueda: Prog. Theor. Phys. Suppl. No. 108 (1992) 133.

(4-46) A. Dönni, A. Furrer, P. Fischer, F. Hulliger, P. Wachter and H. R. Ott: J. Magn. Magn. Mater. 90&91 (1990) 143.

(4-47) J. M. Effantin, J. Rossat-Mignot, P. Burlet, H. bartholin, S. Kunii and T. Kasuya: J. Magn. Magn. Mater. 47&48 (1985) 145.

(4-48) P. Bonville, J. A. Hodges, F. Hulliger, P. Imbert, G. Jéhanno, J. B. Marimon da Cunha and H. R. Ott: J. Magn. Magn. Mater. 76&77 (1988) 473.

(4-49) T. Kasuya: J. Phys. Soc. Jpn. 63 (1994) 843.

(4-50) D. X. Li, A. Oyamada, H. Shida, T. Suzuki, T. Kasuya, A. Dönni and F. Hulliger: Physica B 186-188 (1993) 547.

Chapter 5 Conclusions

We have performed NMR measurements on low carrier semi-metallic compounds Yb-monopnictides. In particular, YbAs has been investigated at low temperatures down to 20 mK.

In all Yb-monopnictides including $YbP_{0.4}As_{0.6}$ and $YbAs_{0.8}Sb_{0.2}$ alloys, the distinct changes of the slopes in K-χ plots are observed. The temperatures where the hyperfine coupling constants change are almost the same in Yb-monopnictides, although the magnitude of the CEF splittings in YbN are about two times larger than those in YbSb. Thus, it is difficult to explaine the temperature-dependent hyperfine coupling constants by the p-f mixing model. The importance of the s-electron for the hyperfine coupling is discussed by comparing the hyperfine coupling constants for Yb-monopnictides with those for the atomic s-electron in pnictogen atoms. The values of the Knight shifts in $YbP_{0.4}As_{0.6}$ measured at the ^{31}P and ^{75}As sites are almost the same with those in YbP and YbAs, respectively. Thus, it is found that the hyperfine interaction in Yb-monopnictides is primarily dominated by the intra-atomic interaction. However, the origin of the temperature dependence of the hyperfine coupling remains unclear.

The temperature dependence of the spin fluctuation rate $1/\tau_f$ is estimated from $1/T_1$. The values of fluctuation rates for YbN, YbP and YbAs are almost the same, reflecting the similarity of physical properties. However, the rates $1/\tau_f$ become larger with changing the pnictogen from As to Sb. From these results, it is confirmed that YbSb is exceptional case in Yb-monopnictides in terms of dynamical aspect. On the other hand, the rates $1/\tau_f$ follows the $\sqrt{T}$ behavior as theoretically predicted for heavy Fermion compounds. Thus, it is found that dynamical properties of Yb-monopnictides are similar to those in heavy Fermion compounds. The difference between $1/\tau_f$ and the half width Γ of quasi-elastic neutron scattering spectra below about 20 K is attributed to the failure of the assumption that the fluctuation rate $1/\tau_f$ and $\chi(q)$ are q-independent.

In YbAs, an NMR spectrum between 0.40 K and 0.61 K consists of two components, indicating that the paramagnetic and the magnetically ordered region coexist. The temperature dependence of the internal field and relative proportion of the ordered region are obtained from these spectra. The magnitude of the internal field is almost

temperature independent throughout the temperature where the paramagnetic and antiferro magnetically ordered regions coexist. Thus, it seems that the phase transition is first order. However, the spin-lattice relaxation rate $1/T_1$ shows a small peak around 0.8 K. The origin of this peak is not clear so far. Further extensive experiments are necessary to clarify the nature of this transition.

Below 0.2 K, Fermi-liquid-like behavior of the spin-lattice relaxation rate given as $(T_1T)^{-1}=2.9$ (s K)$^{-1}$ is observed in YbAs. This large value of $(T_1T)^{-1}$ in comparison with that in non-magnetic reference compound LuAs shows clearly that there is a large enhancement of the number of low energy excitation in YbAs. In order to compare the absolute value of $(T_1T)^{-1}$ for YbAs with those in other heavy Fermion compounds, the Korringa relation for the single impurity region is used. The Korringa relation gives almost the same values for YbAs and $CeAl_2$, though the values of $(T_1T)^{-1}$, γ_N and the Curie constant C are different in the two compounds, respectively. The value of $(T_1T)^{-1}$ for YbAs is explained by the tendency which is found for heavy Fermion compounds. This shows that the large enhancement of the number of low energy excitation in YbAs is due to a large density of state at the Fermi level just like other heavy Fermion compounds. It becomes clear from the microscopic point of view that low carrier semi-metallic compounds Yb-monopnictides are the heavy Fermion compounds with the magnetically ordered ground state.

For YbSb, our NMR measurements clarify the presence of the phase transition around 5 K both in the samples prepared by us and by ETH group. The FWHM of NMR spectra in the ordered state depend on external field stronger than those in the paramagnetic state. There is an additional broadening of an NMR spectrum at the extrapolated external magnetic field of zero in the ordered state. This additional broadening of NMR spectrum seems to be due to the ordering of extremely reduced magnetic moment of about 0.07 μ_B. This can explain consistently the reason why this transition was not observed by neutron diffraction measurements. However, the nature of the ordered state remained unclear. Further experimental and theoretical investigations are required.

List of Publications

(1) NMR study of the phase transition around 5K in YbSb
A. Oyamada, K. Hashi, S. Maegawa, T. Goto, D. X. Li, T. Suzuki, A. Dönni and F. Hulliger
Physica B **199&200** (1994) 42

(2) Study of physical properties of Yb-monopnictides
D. X. Li, A. Oyamada, K. Hashi, Y. Haga,T. Matsumura, H. Shida, T. Suzuki, T. Kasuya , A. Dönni and F. Hulliger
Journal of Magnetism and Magnetic Materials **140-144** (1995) 1169

(3) NQR studies of the structual instabilities in $CePd_2Al_3$
A. Oyamada, H. Tsukada, K. Hashi, S. Maegawa, T. Goto and H. Kitazawa
Physica B **206&207** (1995) 237

(4) Anomalous physical properties of the low carrier concentration state in f-electron systems
T. Suzuki, Y. Haga, D. X. Li, T. Matsumura, E. Hotta, A. Uesawa, M. Kohgi, T. Osakabe, S. Takagi, H. Suzuki, T. Kasuya, Y. Chiba, T. Goto, S. Nakamura, R. Settai, S. Sakatsume, A. Ochiai, K. Suzuki, S. Nimori, G. Kido, K. Ohyama, M. Date, Y. Morii, T. Terashima, S. Uji, H. Aoki, T. Naka, T. Matsumoto, Y. Ohara, H. Yoshizawa, Y. Okayama, Y. Okunuki, A. Ichikawa, H. Takahashi, N. Mori, T. Inoue, T. Kuroda, K. Sugiyama, K. Kindo, A. Mitsuda, S. Kimura, S. Takayanagi, N. Wada, A. Oyamada, K. Hashi, S. Maegawa, T. Goto, Y. S. Kwon, E. Vincent, P. Bonville
Physica B **206&207** (1995) 771

(5) NMR studies of the Antiferromagnetic Heavy Fermion Compound CePdAl
A. Oyamada, K. Kamioka, K. Hashi, S. Maegawa, T. Goto and H. Kitazawa
Journal of the Physical Society of Japan **65** (1996) Supplement B 123

(6) A neutron scattering study of short range spin correlations in Yb monopnictides
K. Ohoyama, M. Kohgi, K. Hashi, A. Oyamada and T. Suzuki
Journal of Magnetism and Magnetic Materials **177-181** (in press)

(7) nuclear magnetic relaxation measurements in Yb-monopnictides
A. Oyamada, K. Hashi, S. Maegawa, T. Goto, D. X. Li, T. Suzuki and
F. Hulliger
Journal of Magnetism and Magnetic Materials **177-181** (in press)

(8) NMR study of the magnetic transition and the Fermi-liquid behavior in YbAs
K. Hashi, A. Oyamada, S. Maegawa, T. Goto, D. X. Li and T. Suzuki
Journal of Magnetism and Magnetic Materials **177-181** (in press)

Acknowledgements

I would like to express sincere thanks to Prof. T. Goto, Graduate School of Human and Environmental Studies, Kyoto University, for his guidance and many advice throughout the course of this work.

I am also very thankful to Prof. S. Maegawa, Graduate School of Human and Environmental Studies, Kyoto University, for his valuable discussions and warm encouragement.

I am very grateful to Dr. A. Oyamada, Graduate School of Human and Environmental Studies, Kyoto University, for his fruitful discussions on heavy fermion compounds.

I express sincere thanks to Prof. T. Suzuki, Department of Physics, Tohoku University, and Dr. D. X. Li, Institute for Materials Research, Tohoku University, for collaboration in preparing the sample and valuable discussions.

I am also very thankful to Prof. M. Kohgi, Department of Physics, Tokyo Metropolitan University, and Dr. K. Ohoyama, Institute for Materials Research, Tohoku University, for their advice especially about neutron experiments.

I would like to acknowledge to Mr. Y. Fujii, Faculty of Integrated Human Studies, Kyoto University, and Mr. H. Nishishita, Department of Chemistry, Kyoto University, for their technical support of the experiments.

I am very thankful to Prof. Y. Oka, Faculty of Integrated Human Studies, Kyoto University, for the X-ray diffraction measurements.

I would like to acknowledge to Dr. A. Dönni and Dr. F. Hulliger, ETH Zürich, for supply of the sample.

I also express sincere thanks to all the members of the Goto and Magawa laboratories, Graduate School of Human and Environmental Studies, Kyoto University, for their assistance and friendship.

Finally, I would like to thank my parents and my friends for their encouragement.